A Z-GRADIENT COIL ARRAY SYSTEM FOR MAGNETIC RESONANCE IMAGING

A THESIS SUBMITTED TO
THE GRADUATE SCHOOL OF ENGINEERING AND SCIENCE
OF BILKENT UNIVERSITY
IN PARTIAL FULFILLMENT OF THE REQUIREMENTS FOR
THE DEGREE OF
MASTER OF SCIENCE
IN
ELECTRICAL AND ELECTRONICS ENGINEERING

By
Soheil Taraghinia
January, 2016

A Z-GRADIENT COIL ARRAY SYSTEM FOR MAGNETIC RESONANCE IMAGING
By Soheil Taraghinia
January, 2016

We certify that we have read this thesis and that in our opinion it is fully adequate, in scope and in quality, as a thesis for the degree of Master of Science.

Ergin Atalar(Advisor)

Yusuf Ziya İder

Nevzat Güneri Gençer

Approved for the Graduate School of Engineering and Science:

Levent Onural
Director of the Graduate School

ABSTRACT

A Z-GRADIENT COIL ARRAY SYSTEM FOR MAGNETIC RESONANCE IMAGING

Soheil Taraghinia
M.S. in Electrical and Electronics Engineering
Advisor: Ergin Atalar
January, 2016

In this thesis, a z-gradient array system for use in MRI is proposed. In MRI scanners, in order to encode the MR signal gradient coils are used. Conventionally, encoding in the z-direction (along the bore of the magnet) carried out using a single gradient coil. Proposed z-gradient coil array is a flexible and novel design to achieve high gradient strength while observing the peripheral nerve stimulation (PNS) limits. The design has a potential to decrease both the complexity and the cost of the gradient power amplifiers (GPA). In order to prove the concept, a three-channel system was designed and built. By using different combination of the generated fields of these channels, effective length of the coil can be modified according to the application. For the same PNS limitations, gradient strength can be increased in a smaller region, hence decreasing the dead-time in most sequences and acquiring images with smaller pixel sizes. In order to proof of concept, this system is designed and implemented in the MRI scanner.

In our preliminary experiment, each channel of the system is composed of two coils with 16 turns each on a cylindrical former with the diameter of 7.5 cm, placed symmetrically about the center with equal current in opposite direction at each side. The overall length of the structure is 245 mm and the current ratio and the distance between the coils optimized such that three sizes of volume of interest (VOI) with more than 95% linearity is achievable. In order to drive each channel independently, three H-bridge GPAs with 30 A current capability at 50 V providing 0.5 $A/\mu s$ slew-rate for the load with 46 μH inductance, 30 μH maximum coupling and 390 $m\Omega$ resistance is built which are controlled digitally by an FPGA ($Xilinx\ XUPV5$) board. Although in this prototype the distance and the current ratio between the coils are the only parameters that were optimized, other parameters of the system can also be optimized according to the different criteria as well.

In addition to the coil simulations, phantom experiments conducted to show the feasibility of this system. 2D coronal slices were acquired for three sizes of VOI; large, mid-size and small volume and different advantages of each mode verified experimentally.

The gradient array is a promising design for the future of the gradient systems in magnetic resonance imaging. In addition to linear fields, gradient array system is also flexible in terms of producing non-linear fields by proper combination of the fields generated by each channel. This is noticeable when higher number of independent channels are used. Gradient array system provides flexible and effective field generation along with less complex amplifier design.

Keywords: z-gradient field, mri gradient coil array, gradient power amplifier.

ÖZET

MAYNETİK REZONANS GÖRÜNTÜLEMESİ İÇİN Z-GRADYAN DİZİSİ

Soheil Taraghinia
Elektrik ve Elektronik Mühendisliği, Yüksek Lisans
Tez Danışmanı: Ergin Atalar
Ocak, 2016

Bu tez'de, MRG'de kullanılmak üzere bir z-gradyan dizi sistemi önerilmiştir. MRG tarayıcılarda gradyan bobinler MR sinyalini kodlamak için kullanılırlar. Geleneksel olarak, z-yönünde kodlama tek bir gradyan bobin kullanılarak gerçekleştirilir. Önerilen z-gradyan bobin dizisi, yenilikçi ve esnek tasarımı sayesinde çevresel sinir uyarımı sinirlerini geçmeden, yüksek kuvvetli gradyanüretmesini sağlar. Bu tasarım gradyan güç yükselteçlerin (GPA) karmaşıklığını ve maliyetini azaltma potansiyeline sahiptir. Bu sistemin kullanılabilirliğini kanıtlamak amacıyla üç kanallı bir sistem tasarlanmış ve üretilmiştir. Bu kanallar ile üretilen manyetik alanların farklı kombinasyonu kullanarak, bobinin etkin uzunluğu uygulamaya göre değiştirilebilir. Aynı sinir uyarım sınırları için,gradyan kuvveti daha küçük bir bölgede artırılabilir. Elde edilen bu yüksek gradyan, çoğu sekansın hızlandırılmasında veya piksel boyutlarının küçültülmesinde kullanılabilir. Bu sistem tasarlanıp birMRG tarayıcıya entegre edilerek kazanımlar gösterilmiştir.

Bu ön çalışmada, sistemin her bir kanal iki bobin den oluşmaktadır. 16 sarımdan oluşan her bir bobin, 7.5 cm çapındaki bir silindirin üzerine, merkeze göre simetrik fakat ters yönde ve eşit akım taşıyacak şekilde sarılmıştır. Yapının toplam uzunluğu 245 mm olmak ile beraber, kanallar arası akım oranları ve uzaklıklar 3 farklı ilgilenilen boyutta (Volume of Interest), %95 doğrusallık sağlanacak biçimde optimize edilmiştir. Her kanalı bağımsız olarak sürebilmek için, 50 V 30 A akım kapasitesi olan, FPGA (Xilinx XUPV5) tarafından kontrol edilen, üç adet H-köprü GPA üretilmiştir. Bu güç yükselteçleri 0.5A/μs akım çıkış oranı ile 46μH öz endüktans ve 30μH karşılıklı endüktans, 390m dirence sahip bir yükü sürebilecek şekilde tasarlanmıştır. Bu çalışmada yalnızca bobinler arasındaki mesafeler ve bobinlerin akım oranları optimize edilmiş olmasına

rağmen, sistemdeki parametreler farklı kriterlere göre de optimize edilebilir. Sargı simülasyonlarına ek olarak, sistemin kullanılabilirliği phantom deneyleri ile de gösterilmiştir. Küçük, orta ve büyük boyutlar olmak üzere 3 farklı boyutta, 2 boyutlu koronal kesit görüntüleri alınarak, her bir modun avantajı doğrulanmıştır.

Gradyan dizisi manyetik rezonans görüntüleme deki gelecek nesil gradyan sistemleri için umut vadeden bir tasarımdır. Doğrusal gradyanlara ek olarak, özellikle çok sayıda dizi elemanı olduğu durumlarda, gradyan dizideki kanalların farklı kombinasyonları ile bir çok çeşit doğrusal olmayan gradyan elde edilebilir. Gradyan dizi sistemi etkin ve esnek gradyan alan üretmeyi daha az karmaşık güç yükselteci tasarımı ile birlikte sağlamaktadır.

Anahtar sözcükler: z-gradyan alanı, gradyan sargı tasarımı, gradyan güç yükseltici.

Acknowledgement

Foremost, I would like to express my deepest gratitude to my advisor, Prof. Dr. Ergin Atalar for his excellent guidance, caring, patience, and providing me with an excellent atmosphere for doing research at UMRAM.

Besides my advisor, I would like to thank the rest of my thesis committee: Prof. Dr. Yusuf Ziya İder and Prof. Dr. Nevzat Güneri Gençer, for their encouragement, insightful comments and encouragement.

I acknowledge my gratitude to Niyazi Koray Ertan for his cooperation and enthusiasm to help and give best suggestions. And also, I am very thankful to Berk Silemek, Sercan Aydoğmuş and Hamed Mohammadi for their help in developing the control method of my system and other colleagues at UMRAM and my friends, for their support and friendship.

Last but not the least, I would like to thank my family: my parents and my sister for supporting me spiritually during my studies and their best wishes throughout my life.

Contents

List of Figures

List of Tables

Chapter 1

Introduction

In this thesis using array of coils to generate a z-gradient field (a linear magnetic field in z-direction) for magnetic resonance imaging (MRI) was proposed. There are two other gradient fields used in MRI to generate linear field in x- and y-directions as well. However, in order to prove the concept of the gradient coil arrays we have chosen the gradient field in the z-direction to demonstrate that it is possible to implement a gradient array system instead of a conventional gradient coil connected to one gradient power amplifier (GPA). In this work an array structure for the z-gradient system designed and experimentally verified.

In order to get a better understanding of the gradient system's functionality, the basic operation of the MRI is explained very briefly here. MRI employs strong magnetic field (B_0) to align hydrogen nuclei spins in one direction. Water contains hydrogen and 70% of human body is composed of water. The number of nuclei that get aligned with B_0 field depends on how strong the magnetic field is. Typical field strength values in commercial scanners are 1.5, 3 and recently 7 T. Hydrogen spin frequency is directly proportional to the magnetic field which can be formulated as $\omega = \gamma B$ where γ is the gyromagnetic ratio and for hydrogen it is 42.58 MHz/T. In MRI, electromagnetic signals are received after applying RF pulses in the form of echoes with a frequency equal to the frequency of hydrogen spins. Gradient coils generate linearly varying magnetic fields in x, y and z

directions which make the frequency of the spins position dependent and hence the image can be reconstructed by taking inverse Fourier transform of the received signal. The subject of this thesis, i.e. the gradient system is responsible for generating linear fields in the x, y and z directions and enables spatial encoding in MRI.

In conventional systems, the gradient field in each direction is generated by copper windings on a cylindrical former with varying spaces between arcs which is driven by one gradient power amplifier (GPA). In order to produce desired magnetic field profile, specific distribution of current density (electric current (A) per unit area (m^2)) should be present on the surface of the gradient coil. Target-field method [1] is one of the recognized methods for the design of the gradient coil in that Ampere's Law is inverted to find the required current for desired field. Obtained continuous current distribution then can be approximated by discrete wire paths appropriately placed on the surface of the cylinder. For the z-gradient coil, they are circular arcs which carry anti-parallel current at two sides, placed close to each other near the two ends of the cylinder and increased spacing toward the center symmetrically [Fig. 1.1], that results in varying surface current density on the cylinder [2]. Various configurations for this kind of magnetic field are described with error limits in [3]. In early designs, the gradient coils were unshielded until actively screened coils were introduced [4], [5] in which a secondary coil is placed outside the primary gradient coil as a shield to nearly cancel out magnetic field outside the gradient cylinder and still maintain linear field inside the bore. It prevents induction of eddy currents on the metal parts outside the gradient cylinder, since they will degrade B_0 field and cause artifacts in image so using shields along with gradient coils is inevitable. This kind of shielding is obtained by using a secondary coil on top of the primary coil with similar wire pattern and a current in opposite direction of the primary coil, hence total inductance seen from the input of the coil will be less than inductance of the primary coil alone. In the conventional systems, once the coil is manufactured no modification can be made on the current density distribution on the coil and therefore the spatial distribution of the gradient field cannot be modified.

Slew-rate (i.e. change in the gradient field strength in unit time) and amplitude

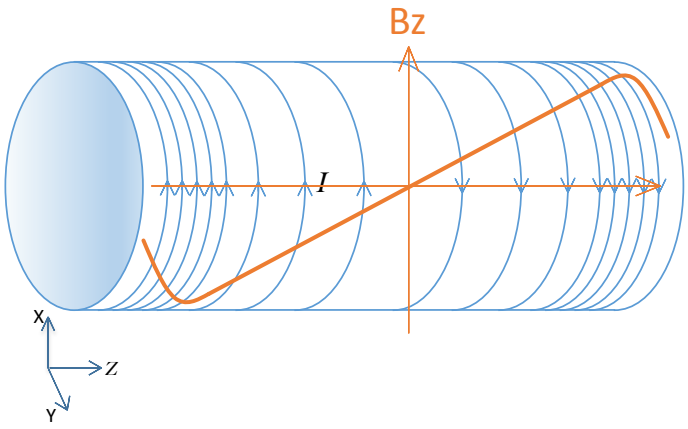

Figure 1.1: Conventional gradient coil for z-direction with discrete wires positioned to approximate current density at those paths carrying same current to generate linear magnetic field inside the desired region.

of the gradient fields are two important parameters that should be maximized. The higher gradient field strength, the faster data acquisition speed. High slew-rate decreases the dead-time in most sequences. High gradient field allows taking images with smaller voxel sizes [6]. High performance gradient system has advantages in special sequences such as diffusion weighted imaging which requires very strong gradient to obtain the desired b-values and echo planar sequences produces better image quality with high performance gradient systems. Some trade-offs may be considered between gradient system parameters. For example in order to have higher magnetic field, under determined power limitations, larger inductance is needed. But on the other hand, slew-rate which is another key factor, will be degraded. Also note that high slew-rate and high gradient amplitude have different applications. So improving the properties of the gradient system is essential, specially the slew-rate and gradient strength.

Body gradient coil has large inductance in the order of several hundred μH (600 μH), thus for high slew-rates, high voltage levels are required [7]. Also high current is flowing in the gradient coils to generate strong magnetic fields. GPA has to provide current with large amplitude to get image and high voltage for required slew-rate and fast imaging [8]. These values in the Siemens 3T Trio MRI scanner at UMRAM are 625 A maximum current and 2000 V maximum voltage to get 200 mT/m/ms slew-rate. Analogue amplifiers initially employed in early

gradient systems, but semiconductor losses limited achievable power and duty cycles. Digital amplifiers, i.e. the amplifiers that are controlled by Pulse Width Modulation (PWM) do not suffer from these losses, thus become typical drivers for the MRI gradient coils. In order to meet the high power requirements, different combination of parallel or stacked H-bridge structures have been proposed [9, 10]. Combined parallel and stacked configuration in [11] shows good performance in terms of power and bandwidth demands but this design technique is expensive and complicated. In addition the power losses are critical and cooling networks are mandatory to dissipate heat in driving systems and coils. Considering these requirements, GPAs become one of the important and also expensive parts in gradient systems.

Rapidly changing of the magnetic fields in the gradient systems induce electric field in the body. For high amplitude which is present at the periphery of the body and sufficiently long duration, this electric field can stimulate periphery nerves. This effect is called Peripheral Nerve Stimulation (PNS) and starts from tingling and muscle twitching to intolerable pain. In 1990 Mansfield et al. [12] pointed out that under specific total magnetic value, PNS is in fact independent of the dB/dt which has been confirmed in [13] and [14] as well. Equation 1.1 [15] describes the relation between magnetic field value at stimulation (B_m) and rise time (t_r):

$$B_m = \frac{B(\infty)}{(\frac{\tau_m}{t_r})(1 - exp(\frac{-t_r}{\tau_m}))} \tag{1.1}$$

$B(\infty)$ is the threshold level under which there will be no nerve stimulation for any slew-rate. This value is 5.9 mT which is empirically verified in [14] as well. τ_m is the time constant of the membrane and it's selected to be 170 μs in the literature which results in fitting this expression in all cases of the whole-body gradient coil magneto-stimulation data [14, 16]. Figure 1.2 depicts magnetic field amplitude with respect to the rise time. The region under the plotted line is safe in terms of the PNS and below certain magnetic field value ($B(\infty)$), stimulation will not occur irrespective of the rise time or slew-rate. There are some studies [16, 17] that measure nerve stimulation experimentally with similar results supporting PNS equation [Eq. 1.2]. They have also indicated that $\mid B \mid$ -modulus of the magnetic vector- is more related to PNS rather than imaging component of the

gradient field (B_z) [17]. Therefore by considering the mechanism behind this effect, gradient systems design can be modified to keep PNS as low as possible.

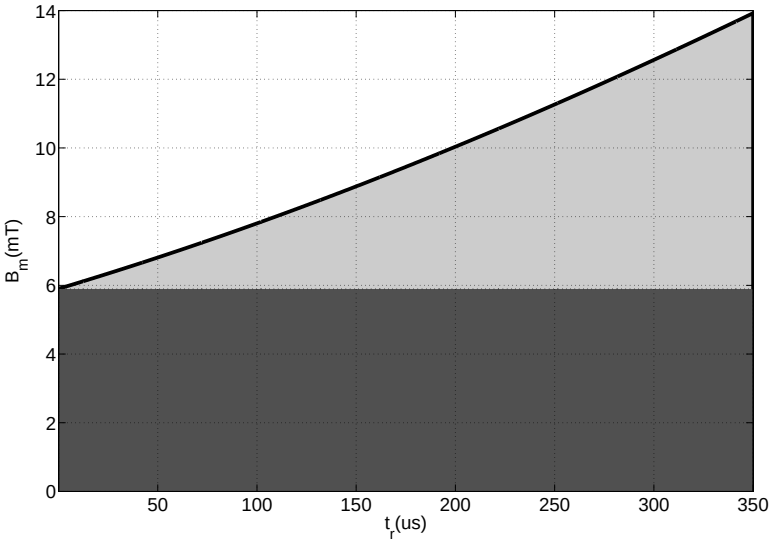

Figure 1.2: Magnetic field at stimulation vs. rise time [Eq.1.1] indicating PNS won't occur under specific magnetic field amplitude regardless of its frequency or rise time (dark gray area).

There have been some studies focusing on producing different sizes of volume of interest (VOI) and benefit form properties of each mode. In mid 1990s patents with the principle of variable VOI called "switchable gradient systems" were filed [18,19]. Harvey and Katzelnelson built first so called "twin coil" gradient modular system [20–22] in which two sizes of VOI were achievable, smaller one with high gradient strength and high slew-rate observing PNS limitations as needed in neuro and cardiac imaging and larger volume with properties of conventional systems in terms of the slew-rate and amplitude for the whole body imaging. Later on some works patented with the title of continuous scaling of VOI [23, 24]. In 2002, prototype of continuous varying volume of linear region designed and built [25] in which desired size can be changed by superposition of the field created by basic and supplementary coils. As mentioned above, ability to change size of VOI in order to benefit from properties of each mode has been considered as a research topic for about two decades.

In this thesis an array configuration for the z-gradient system is introduced that

addresses some limitations of the conventional systems and also shows flexibility in terms of generating sizes of VOI adopted to different applications. Another way of achieving desired current density is applying required currents to the coil windings at each section namely channels, along the coil surface to achieve desired current density rather than varying the spacing between the current arcs. In this way by using different combination of these channels, variable VOI is achievable. There are three independent channels and three different VOI is available in the proposed design. For the large VOI all of the channels, for mid-size volume two of them and for small region one channel is driven, hence power consumption can be optimized for specific application which is critical in the gradient systems with high power demands. Since the PNS is fundamentally related to the magnetic field amplitude [13], higher slew-rates and faster imaging will be possible in smaller VOI with the same field amplitude level. Each channel has to be connected to the independent gradient amplifiers. Home-built one stage H-bridge gradient power amplifiers (GPAs) are designed and implemented in order to integrate with the MRI system and measure the generated field. Each channel has lower inductance compared to single conventional coils which means to achieve same slew-rate, amplifier design will be less demanding due to lower voltage requirements. It is believed that making several amplifiers with lower VI capabilities is cheaper than one amplifier with combined VI levels. Three independent channels are controlled digitally by an FPGA ($Xilinx\ XUPV5$) by providing the GPAs with required PWM control signals. Each part of the proposed system is described accordingly in the next chapter followed by the results in chapter 3 and discussion and conclusion in the last chapter. The next chapter begins with the theory behind the z-gradient coils.

Chapter 2

Methods

In this chapter, z-gradient array design, the array of power amplifiers for the coil and their control system are explained. The properties of the conventional z-gradient coil is briefly described in the first section together with the idea of obtaining desired magnetic field by dividing the coil into independent current loops. In order to drive gradient coils, different combinations of so called H-bridge amplifiers are used in conventional systems to feed them with desired current and voltage levels. In order to prove the concept, one stage amplifier designed and built and its specifications are discussed in the next section. Control system requirements and the applied method is described in Section 2.3. This system is based on the FPGA and VHDL programing language. Also experimental verification of the whole system was conducted which is explained in the last section. This chapter essentially covers the theory behind the gradient array system.

2.1 Z-Gradient Coil Array Design

In the conventional z-gradient coil design all the current arcs are driven in series and the same current is flowing through the entire coil. This coil has large inductance in the order of several hundred μH and to achieve desired slew rate

($> 2A/\mu s$) amplifier with high voltage ($\sim$ 1000 V) capabilities is required. Also in the conventional z-gradient systems, once the coil is built, no modifications can be made for the current density distribution on the surface of the coil. On the other hand, in some applications higher gradient field for a smaller region is required, which may be over the power limitations or may not be an efficient way to drive the whole coil and benefit from only a small portion of the linear field generated by the coil. Hence the standard z-gradient coils are not so flexible and effective in terms of generating required magnetic field.

Another way of achieving the same current density distribution is to divide the coil into several segments and drive them with required current rather than spacing between arcs. This results in the array design which adds more flexibility in generating desired current density distribution that is the main contribution on in this thesis. Furthermore, if a solenoid is divided into multiple segments, required voltage and power levels to drive each part will be divided accordingly. This may potentially reduce the complexity and the cost of the amplifiers. The coil array configuration can address some limitations of the conventional systems by adding more flexibility and effectiveness to the standard systems.

As a simple preliminary design, the configuration that has been investigated in this thesis has three channels. Also, since the power necessary to energize the coil is proportional to the fifth power of the coil radius [26], small coil size (D=7.5 cm) is selected for ease in implementation and reduction of the cost. Each channel has winded wires adjacent to each other making two groups placed symmetrically about the center in z-direction, with anti-parallel currents [Fig. 2.1]. One of the advantages of this design is ability to drive each channel by different currents, thus current density distribution on the surface of the cylinder can change. This gives remarkable flexibility in terms of generating sizes of VOI according to the application. As a result, considering the PNS limitations, as described in the introduction, being under threshold magnetic field, slew-rate can be increased. This is achievable through decreasing the size of VOI while maintaining the field amplitude as depicted in Fig. 2.1. Different advantages of the coil array is investigated by using a three-channel system and small coil size compare to standard coil sizes as preliminary design.

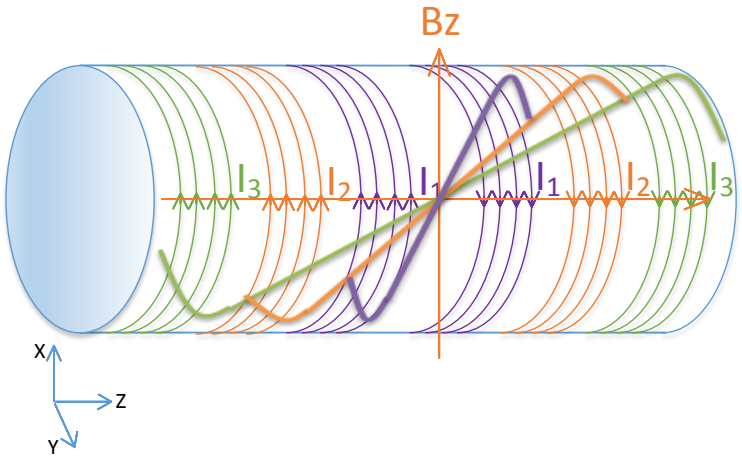

Figure 2.1: Proposed array configuration for the z-gradient coil gives flexibility in generating the desired current density for each section hence improving performance in terms of PNS by linear magnetic field generation in smaller regions.

In order to obtain linear region with variable sizes using coil array, there are many parameters that contribute to the magnetic field properties such as number of the turns, spacing between the loops and wires, ratios of current between the channels, wire paths and etc. In our gradient coil array design, we have fixed some parameters such as the diameter of the loops, turn number, radius of the wire. The distance and the current between the channels optimized to get the desired linear field. The distances between the channels were found empirically and optimized current ratio obtained by minimizing the root mean square error between the generated field and the desired one. In the coil prototype, each of two groups in one channel is composed of 16 loops with 2.1 mm width wire on a 75 mm diameter cylindrical structure [Fig. 2.2]. The distances between the channels and their currents I_1, I_2 and I_3 are determined using a program written in Matlab (Mathworks, Natick, MA) by using the *Biot-Savart* law for a linear region inside the coil in the z direction with at most 5 % field error. The spacing between channels are calculated such that by applying different current ratios for channels, three VOI in large, mid- and small sizes are achievable. Driving all the channels in order to get largest VOI extended along the z-direction, driving middle and inner channels for smaller VOI and as the third case, when only the inner coils is used, smallest linear region will be available. This is advantageous when higher gradient is needed in a small volume of interest and not driving the

whole coil but only the most inner pair with desired current level and still remain under maximum allowable magnetic field in order to avoid the PNS. Distance between loops of most inner pair is roughly determined in a way such that they be capable to generate a linear field with at most 5 % nonlinearity when no current is passing through the other coils (i.e. $I_2 = I_3 = 0$). This distance is directly proportional to the loop radius by a coefficient of 1.73 known as Maxwell pair [27]. Once the determined current ratio is maintained, desired magnetic field strength will be realizable by corresponding current levels applied to the coils. So in this design optimizing the current ratio and the distance between the channels play an important role in generating magnetic field with specific characteristics while the other parameters kept constant.

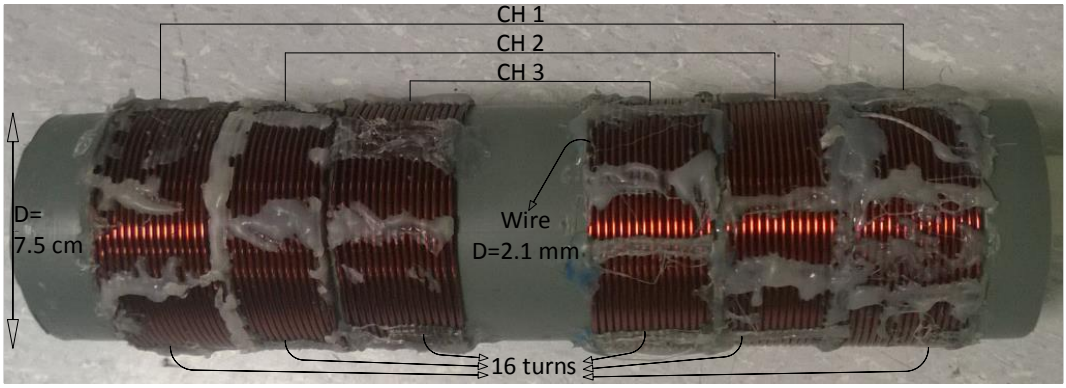

Figure 2.2: The z-gradient coil prototype with specified turn number for each channel and former diameter.

The electrical characteristics of the coil are required in order to model it as the load of the amplifier. Using the finite-length solenoid formula [Eq. 2.1] [28], where μ_0 is permeability of free space, N is the number of turns, a is the coil radius and l is length of the coil, the inductance of each group calculated to be $21\mu H$ and neglecting the mutual inductance between two groups in each channel (since they are not close to each-other), total inductance of each channel will be $42\mu H$. Measured value of the inductance for all channels are almost equal and it is $46\mu H$. The mutual inductance between coils n and m (M_{nm}) is the proportionality constant that relates time rate of change of the current in coil m (I_m) to the time rate of change of magnetic flux (ϕ_{nm}) in coil n [Eq. 2.2] which can

also be rewritten as $M_{nm} = \frac{N_n \phi_{nm}}{I_m}$. This mutual inductance depends only on the geometrical properties of the coils and the distance between them and determines the amount of the induced emf in the other coil stimulated by the current coil. By using the *reciprocity theorem*, one may show that the mutual inductance between two coils are equal $M_{nm} = M_{mn}$. Although there are methods to theoretically calculate the mutual inductance between coaxial circular coils [29], but here in order to find accurate values, the coupling is measured between the channels. This is done by applying a time varying current to one channels and measure the induced voltage from the other channel to find the mutual coupling between them. The mutual inductance between the outer and the middle channel (M_{12}) measured to be about $30\mu H$, less than $1\mu H$ between the inner and the outer channels (M_{13}) and about $21\mu H$ between the middle and the inner (M_{23}) coils. Total resistance of the coil is composed of DC and AC resistance. The AC resistance in return arises as a result of the *proximity effect* in time varying currents. Since there are long connecting cables with soldered connections to the coil, the total resistance is found empirically for each channels as well. This is done by connecting each channel to the amplifier and measure the current resulting from duty cycle calculated from the resistance. When the measured current matches the expected value, it indicates that the resistance is actual resistance value for that channel which found to be about $390m\Omega$. Because of the high current amplitudes passing through the gradient coil, their temperature increase which results in higher resistance value. In the conventional gradient coils, there are cooling systems to decrease this effect as much as possible. In the proposed gradient coil since this increase in temperature was under 50°C, experiments were conducted after some time letting the system to reach a stable state. So in this work the electrical characteristics of each channel are measured to find the actual values to use in the design of the amplifier control signal.

$$L \approx \frac{10\pi\mu_0 N^2 a^2}{9a + 10l} \tag{2.1}$$

$$N_n \frac{d\phi_{nm}}{dt} = M_{nm} \frac{dI_m}{dt} \tag{2.2}$$

This z-gradient coil is both force and torque balanced considering main field (B_0). The force at each point is canceled out by the same amount of force in

the point in front of it on the same loop but in the opposite direction. The PVC cylinder used as the former of the coil, provides sufficient durability to tolerate these forces.

2.2 Gradient Power Amplifier (GPA)

In order to generate gradient fields for imaging purposes, high current levels in the order of several hundred amperes are required to drive gradient coils for each x, y and z direction. For a body size gradient coil, both the inductance of the coil which can be in the range of several hundred μH, and the rise time requirements of the gradient field for fast imaging and also to prevent signal loss, require more than a thousand of volts. Pulse Width Modulation (PWM) amplifiers have been a standard amplifier type to drive MRI gradient coils [30]. In order to meet these high VA requirements, parallel and stacked bridge structures have been combined. Dividing the coil into channels results in lower inductance value for each channel compare to conventional coil hence high voltage requirements reduce and possibly simpler configuration suffices. In this thesis, GPA prototype for small coil dimensions have been designed and built which will be covered in this section.

2.2.1 H-bridge Concept and Design

Gradient fields in the MRI are required to be switched ON and OFF rapidly and in extreme cases, since the field is directly proportional to the current, waveform of the current passing through the coil gets form of a trapezoid instead of ideal square shape since applying infinite voltage to get instant change of the current in an inductive load is impractical according to the basic voltage-current equation of an inductor. Eq. 2.3 gives required voltage for each coil of three channel array

ignoring the coupling between the channels.

$$\begin{bmatrix} V_1 \\ V_2 \\ V_3 \end{bmatrix} = \begin{bmatrix} L_1 & M_{12} & M_{13} \\ M_{21} & L_2 & M_{23} \\ M_{31} & M_{32} & L_3 \end{bmatrix} \begin{bmatrix} \frac{di_1(t)}{dt} \\ \frac{di_2(t)}{dt} \\ \frac{di_3(t)}{dt} \end{bmatrix} + \begin{bmatrix} R_1 & 0 & 0 \\ 0 & R_2 & 0 \\ 0 & 0 & R_3 \end{bmatrix} \begin{bmatrix} i_1(t) \\ i_2(t) \\ i_3(t) \end{bmatrix} \tag{2.3}$$

The current in rising/falling sections induce current in other coils since the it's changing with respect to the time. It doesn't occur in the flat top section with constant current ignoring the current ripples inherent at the output of PWM amplifiers. So in order to compensate for the coupling, since the current direction is the same in the coupled coils, we have to apply higher absolute voltages to achieve correct and desired slew-rate for three channels. As mentioned before, mutual inductance between two channels are equal to each other. If we assume small resistance of the inductor, required voltage to get the desired current waveform is shown in Fig. 2.3. For a fixed load, slew-rate value which is maximum current (I_0) ratio to the rising or falling time (t_r, t_f), plus the voltage across the resistance, is a determining factor for the required maximum voltage. In this design since

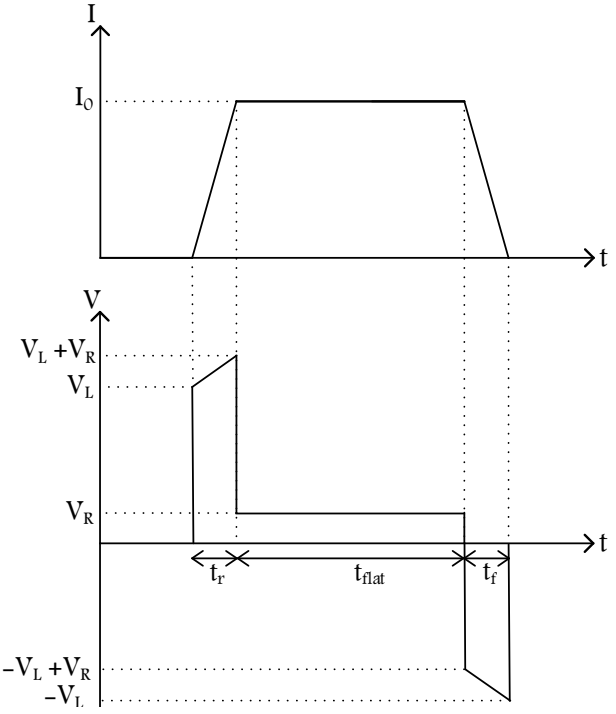

Figure 2.3: Typical gradient current waveform and required voltages to generate it.

the rising and falling times are kept equal between three channels and are equal to 60 μs which is adjustable, slew-rate is variable and it depends on the required current values and the maximum is 0.5 $A/\mu s$ for our load. For the flat top part (t_{flat}) in which the current doesn't change with the time, the total resistance is determining factor to generate the current according to the applied voltage. Although the electrical characteristics of the coil was not considered for the power efficiency, the range of the inductance and the resistance of each channel tried to be such that the GPAs can drive them with desired values for maximum current and slew-rate as mentioned above. Since the resistance value is small and in the range of $m\Omega$, small voltage level (V_R) will be sufficient to generate desired amount of current in the coil. For the maximum 30 A current, required voltage levels are about maximum 23 V and 11.7 V for rising/falling edge and flat top, respectively when there is no coupling between the channels and considering the highest mutual inductance, required maximum voltage is about 45 V. The definitions and formulas stated here are used in the design considering a trapezoidal waveform of the load current.

H-bridge amplifier with PWM consists of four switches delivering required voltage level to the inductive load [Fig.2.4] by the appropriate duty cycle specified by the control signals. Assuming all the MOSFET switches are ideal, pulses with both positive, negative and zero amplitudes with variable duty cycles can be generated which is depicted in Fig. 2.5 for a typical trapezoidal waveform. High inductance along with series low resistance, which is the case in gradient coil modeling, takes the integral of the voltage across it in time, hence required voltage is calculated directly proportional to the duty cycle of square wave in PWM. Considering this, for different current segments [Fig. 2.3], different voltage levels and consequently different duty cycles for PWM signals will be required which is depicted in Fig. 2.5 (c). Desired duty cycle is equal to the ratio of the required load voltage and the line voltage [Eq. 2.4]. This varying duty cycle is generated by FPGA which is covered in the next section.

$$Duty\ Cycle\ \% = \frac{V}{V_{LI}} \times 100 \tag{2.4}$$

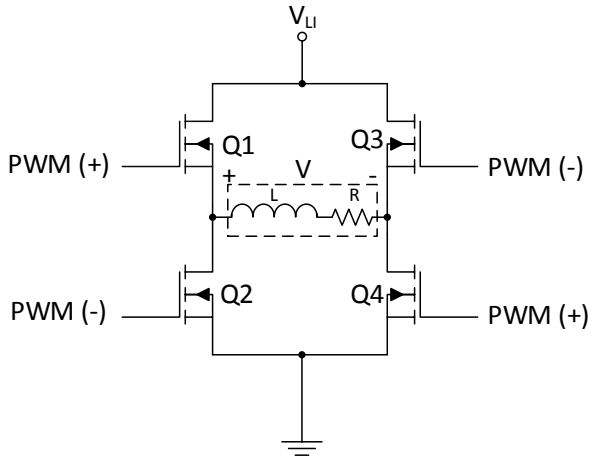

Figure 2.4: H-bridge amplifier driving the coil modeled with an inductor and total DC and AC resistance consisting of four switches with the line voltage V_{LI} and control signals responsible for applying either positive (+) or negative (-) voltage on the load.

Desired net duty cycle is achieved by $Duty\ Cycle = D^+ - D^-$ where D^+ is the duty cycle of pulses turning $Q1\&Q4$ ON and D^- is the duty cycle of pulses turning $Q2\&Q3$ ON [Fig. 2.4]. For example when $Q1\&Q4$ are ON, V^+ with respect to the ground is V_{LI}, and when $Q2\&Q3$ are ON, V^- with respect to the ground is V_{LI} and $V = V^+ - V^-$ [Fig. 2.5], keeping in mind that $Q1$ and $Q2$ or $Q3$ and $Q4$ are never ON at the same time, so overlapping is not allowed. As an example if desired net duty cycle is 0.8 in negative direction, we should have $D^+ = 0.1$ and $D^- = 0.9$ considering equal increase/decrease steps for both D^+ and D^- which is shown in Fig. 2.5 and for zero duty cycle $D^+ = D^- = 0.5$. In addition, center aligned PWM in which two pulses with duty cycle D^+ and D^- are aligned symmetric in the center of their pulses, have the advantage of minimized ripple current and less harmonics. The duty cycle of the control signals determine the effective duty cycle on the load.

Figure 2.6 is the schematic of h-bridge circuit that we use to drive our coils. There are four switches ($Q1, Q2, Q3$ and $Q4$) that are implemented by using N-type MOSFET IRFP 250n, which are turned on and off two by two in crossed form resulting in bidirectional current flow in load. These sequences are controlled by PWM pulses from an FPGA. Gate driver signals of high side MOSFETs ($Q1$ or

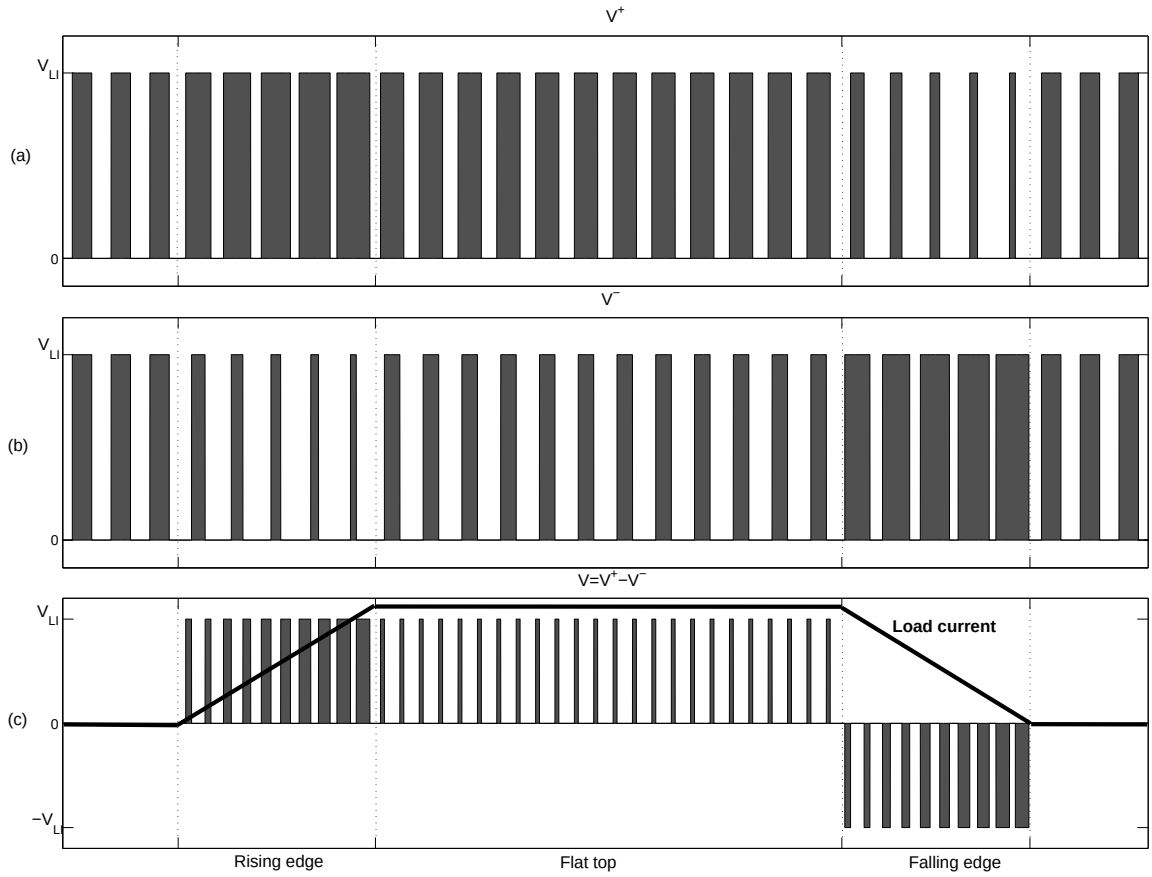

Figure 2.5: Typical PWM pulses for right (a) and left (b) half bridges required to get desired duty cycle on the load to get the trapezoidal load current (c).

$Q3$) are referenced to floating voltage of the source and since that is equal to line voltage V_{LI} when the switch is on, some mechanism should be applied in order to get higher voltage than V_{LI} at the gate. In this design, bootstrap method is used which is simple and inexpensive and is composed of two resistors $R1$, $R3$ and $R9$, one diode $D1$, one Zener diode $Z1$ and one capacitor $C1$. Since a full H-bridge is composed of two half bridges, all the descriptions are valid for the other half as well. At the beginning the capacitor starts to be charged through the resistors and the diode and then according to the PWM signal, the voltage of the capacitor will be applied on gate and source of the MOSFET by driver. $R9$ is the bootstrap start-up resistor which charges the $C1$ immediately after power-on and starts-up the bootstrap circuit. The time constant is equal to $\tau = (R1 + R9) \times C1$. Low values of this resistor can be responsible for power dissipation when $Q1$ is ON,

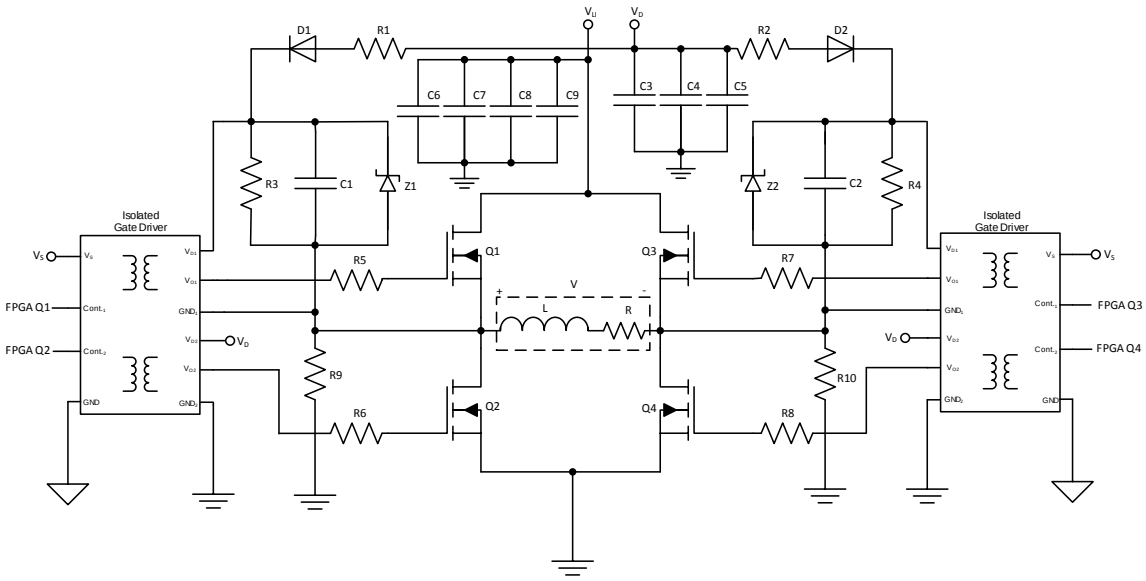

Figure 2.6: Circuit diagram of H-bridge GPA to drive our costume gradient coil.

therefore resistance value of 750Ω has been used as a compromise between short time and low power loss. $R1$ limits bootstrap current for charging the $C1$ with reasonable voltage drop, the value for that is 10Ω for this design, considering maximum dc current of $30mA$ for the gate driver [31]. Considering maximum acceptable voltage drop ($\Delta V = 0.5$ V), driver supply current ($22mA$) and ON duration of MOSFET (max. $60\mu s$) while driving the high side switch, $C1$ is calculated to be $C1 = I_c \frac{\Delta T}{\Delta V} = 2.2\mu F$. When high side MOSFET $Q1$ turns ON, $D1$ will be reversed biased, therefore capacitor voltage will be applied across gate and source of the MOSFET by gate driver chip. $Z1$ Zener diode is for over-voltage protection when load inductance and parasitic capacitance start to resonate and cause over-voltage condition on bootstrap capacitor which is clamped by 13 V Zener diode. $R3$ discharges $C1$ after power-off. Gate of low side MOSFETs ($Q2,\ Q4$) are referenced to the ground and therefore there is no need to use bootstrap circuit for them.

Gate driver resistors are selected according to the desired switching time (t_{sw})of the MOSFETs and lower voltage ringing. There is a trade-off between shorter switching time and overshoot in rising/falling edges of the pulses. Eq. 2.5 gives the required value considering switch time (t_{sw}), in which I_G is gate current, $V_{GS(th)}$ is threshold voltage of the MOSFET (= 4 V), Q_g is required total gate

charges for the MOSFET to make it ON (= 75 nC). R_{out} is about 4 Ω for our gate driver. Short switching time (t_{sw}) is desired and we chose it to be 90 ns which falls into capabilities of the MOSFET. R_G calculated to be about 5.6 Ω.

$$I_G = \frac{V_D - V_{GS(th)}}{R_G + R_{out}} = \frac{Q_g}{t_{sw}} \tag{2.5}$$

Practically 15 Ω for high side gates and 12 Ω for low side gates found to be suitable in this aspect.

Parallel $C6$-$C9$ capacitors of 1000 μF with low ESR for low IR drop, are used as filters to prevent damage to the power supply because of high current peaks in the load. $C3$-$C4$ capacitors are for filtering purpose for bootstrap circuit with values about 470 μF. V_s is about 4.5 V and V_D is about 12 V required for gate driver. V_{LI} is determined according to the load and desired rise time of the current which is covered earlier. $ADuM$ 7234 has been chosen as the gate driver which possesses isolation between independent inputs and outputs, allowing high voltage peaks (±350) relative to the input. PWM control signals are generated by $XilinxXUPV5(ML509)$ Evaluation Board in CMOS 3.3 voltage level which is accepted by $ADuM$ 7234 as high input logic so no need to level shifter circuit in the input of this driver. Fig. 2.7 shows the three channel array coil connected to the GPAs which are controlled by an FPGA.

There are some important considerations in operation of this amplifier in practice. Turning ON and OFF sequences of high side and low side switches are interleaved and they shouldn't become ON at the same time. When control signal for low side switch goes high at the time that control signal for high side switch goes down, since high current flows through high side switch, it doesn't become open circuit instantly and an overlap occurs in transition between ON/OFF states of switches which results in shoot-through which is grounding line voltage (V_{LI}). Hence a small delay of about 40 ns for this design provided digitally by FPGA between OFF signal of high side switch and ON signal of low side switch can prevent this shoot-through. This problem is not noticeable turning OFF the low side switch and turning ON the high side switch, so that delay is applied between only one edge of the control pulses. Therefore four independent control signals for each switch is required which is generated by FPGA. Voltage ringing may

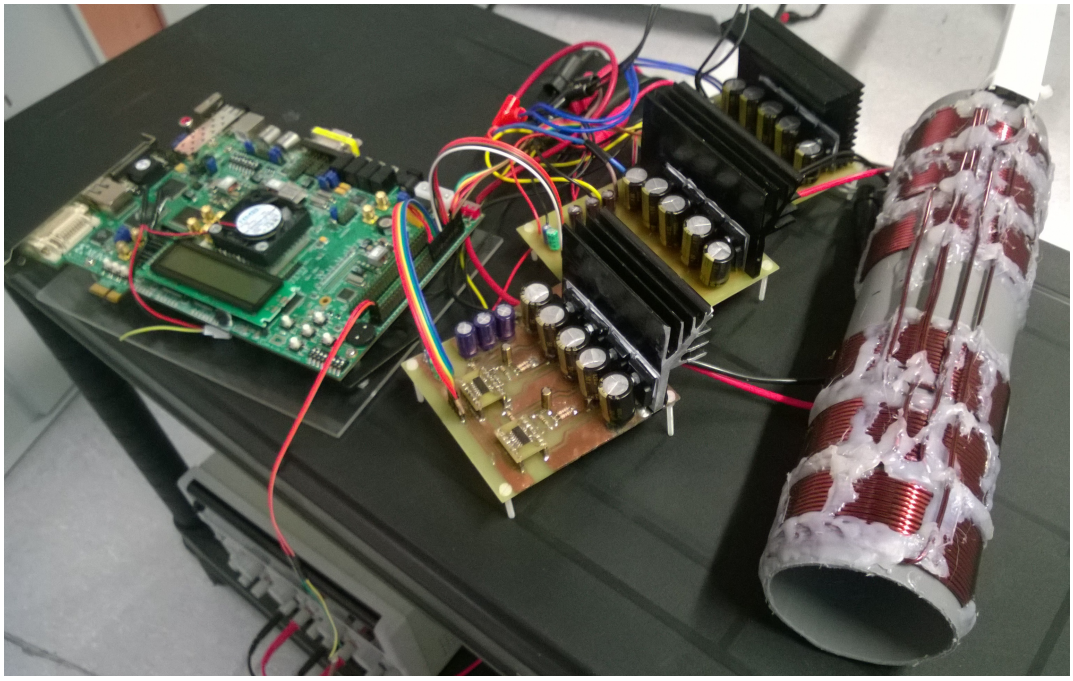

Figure 2.7: Winded gradient coil along with custom made GPAs controlled by an FPGA which is synced with MRI.

appear in switch nodes due to inside capacitor and inductor of the switch devices and connections. This can be reduced by careful PCB design including minimize node distances, and gate/bootstrap resistors to slow down the turn ON/OFF of the control switches. Proper and separate grounding is crucial. All the output side high current grounds should be kept distinctly separated from the logic signal ground that comes from FPGA to the driver which is achieved thanks to the isolated gate driver ($ADuM$ 7234) as well. Since prompt control of high VA levels is required in gradient systems, these practical issues become very crucial in the design and operation of the system.

2.2.2 GPA and Coils Prototype

Fig. 2.8 is GPA prototype with heat sink attached to the switches to dissipate conduction and switching losses of the MOSFETs. The dimension of the PCB can get smaller by optimal PCB design as well. For this work three of this prototypes built and independently controlled by an FPGA. In this way, all three channels

can be driven by each GPA with desired current value timings.

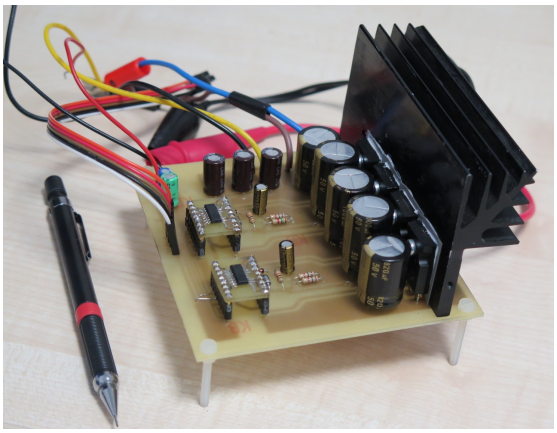

Figure 2.8: GPA prototype with isolated logic and high current side grounds.

Coil prototype is depicted in Fig. 2.7. Over all length of the coil prototype (=264 mm) was 16 mm larger than the simulated coil because of the small unwanted spaces between arcs.

Designing the gradient coil, we didn't optimize it for efficient operation with the GPA. In order to get higher efficiency, load resistance should be much higher than the source (amplifier) resistance [Eq. 2.6]. Since our working frequency is not high but large power rate is delivered to the load, efficiency is of concern rather than maximum power transfer. Aimed at testing and measuring efficiency of the amplifier close to its margins, we built another one channel coil with higher resistance and inductance [Fig. 2.9] with linear magnetic field at its center. It has 80 turns of wire with 0.825 mm diameter at each side winded on a former with 75 mm diameter, starting from ± 30 mm z positions. Measured inductance and resistance of this coil are 730 μH and 1.82Ω whereas they are 46μH and 390$m\Omega$ (without connecting cables) for designed gradient coil, respectively.

$$\eta = \frac{R_{load}}{R_{load} + R_{source}} \tag{2.6}$$

For this work we didn't use any filters since our aim was measuring the gradient magnetic field which was not effected noticeably with the ripples present at the

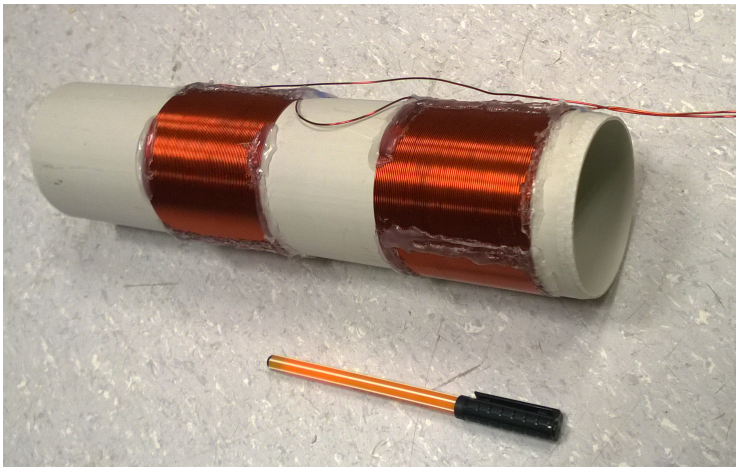

Figure 2.9: Gradient coil with high inductance and impedance in order to test the GPA and measure its efficiency.

output current of the switching amplifiers.

2.3 Control Signals and FPGA Implementation

In order to generate control PWM signals to drive the switches, FPGA which was programmed by VHDL, is used. There are three independent channels each of which requires four separate control signals. Ideally two identical but reverse signals will be sufficient to drive a half-bridge amplifier, but since there should be an delay after turning OFF the high side and turning ON the low side MOSFET to avoid shoot-through, we implemented independent control signal for each switch, hence for three channels we need 12 output signals generated separately. Initially *Basys* 2 Evolution Board used to control one channel, but the resources were limited for three channels so $XilinxXUPV5(ML509)$ is selected to increase the flexibility of the control system, along with the developed user-interface which is depicted in Fig. 2.10. Load specifications, required current amplitude and durations can be specified through this user-interface. The host pc is connected to the FPGA with RS-232 serial communication standard and after entering the inputs the control signals are generated and sent to the amplifiers by the FPGA.

Following is the description of the main function of the VHDL code and its utilities. For each channel, desired duty cycle of rising, flat top and falling sections of the current is calculated independently considering load specifications and line voltage (V_{LI}) as described in GPA section. Fig. 2.11 shows flow chart of generating control signals for $Q1$ and $Q3$ switches as an example. As described in section 2.2.1, desired Duty Cycle is achieved by subtraction of D^+(Duty Cycle of control signal for $Q1$) and D^-(Duty Cycle of control signal for $Q3$), hence each of these control signals contributes to half of desired Duty Cycle and consequently for each edge of one PWM pulse in if statement, quarter of the desired Duty Cycle is considered.

In order to PWM to operate, period of the each pulse should be several folds less than time constant of the load to prevent the current generated in the inductor being discharged through the total resistance of the coil in the duration of "$1 - duty\ cycle$". Time constant of our load ignoring coupling between channels, is about 120 μs and the PWM pulse period is chosen to be 20 μs for each half-bridges, so effective pulse period that load sees will be 10 μs. In this design, coupling between the coils is effecting the time constant and makes it longer, hence doesn't violate the required operation conditions. On the other hand, there is a trade-off between PWM switching frequency (or PWM period) and PWM resolution, to get higher resolutions required for wide control band width, switching frequency decreases for a fixed clock period which makes the output difficult to filter and also *time constant* of the load puts a limitation on it. For this system 11 bits resolution and about 50 KHz switching frequency are compromised values for 100MHz FPGA clock frequency. So PWM frequency is selected according to the load specifications and required control bandwidth.

To calculate desired duty cycle some mathematical operations such as multiplications and divisions with fairy large numbers were needed which was very difficult to do with VHDL and in some cases wrong outputs were generated. In order to perform it in a precise manner, MicroBlaze design is used. Therefore after applying required operations to the parameters specified by user-interface in this core, results are sent to FPGA to generate pwm signals.

In order to integrate this system with MRI, a trigger input has been implemented in FPGA to get the synchronization signal from the MRI and start the outputs after determined delay time considering system pulse sequence.

2.4 Phantom Experiment

The system was placed inside a Siemens 3T Trio scanner and in order to measure the generated field, phase of a gradient echo image was obtained using scanners original gradient coils after applying a small pulse using the developed gradient array. In order to block high frequency noise, an LC low pass filter used in current path immediately before Faraday's cage. A $NaCl$ and $CuSo_4$ doped water used as phantom with 5 cm diameter. In order to experimentally verify properties for each size of VOI, coronal 2D slice selection of a cylindrical phantom (Fig. 2.12) was acquired separately. System gradients and body coil were used to readout. In these experiments, since RF coil array wasn't used, the phantom was shielded in order to prevent excitation of unwanted regions of the phantom as shown in Fig. 2.12. Pulse sequence used for this experiment is depicted in Fig. 2.13. Slice selection is performed using custom z-gradient coil while RF signal is transmitted followed by a negative lobe. The area of the negative lobe should be half of the positive lobe in order to correct dephasing of the proton spins with maximum negative amplitude to minimize the duration to reduce signal loss due to $T2^*$ effect as much as possible. For coronal (xz plane) read-out, system gradients in x and y directions are used to sample the k-space. The images obtained and with different parameters revealing properties of each mode and presented in the next chapter.

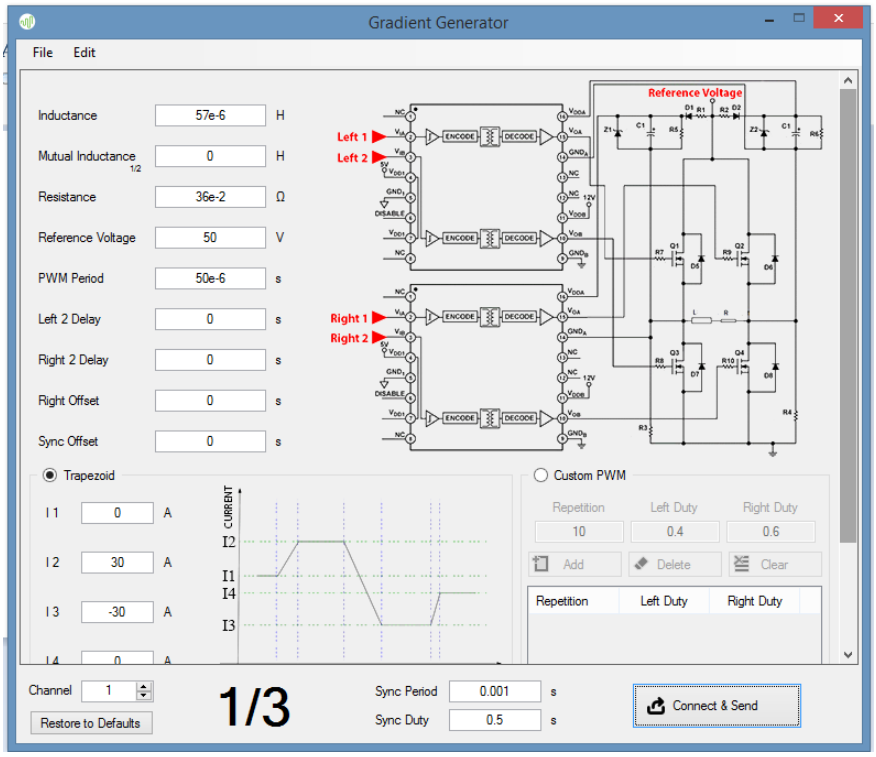

(a)

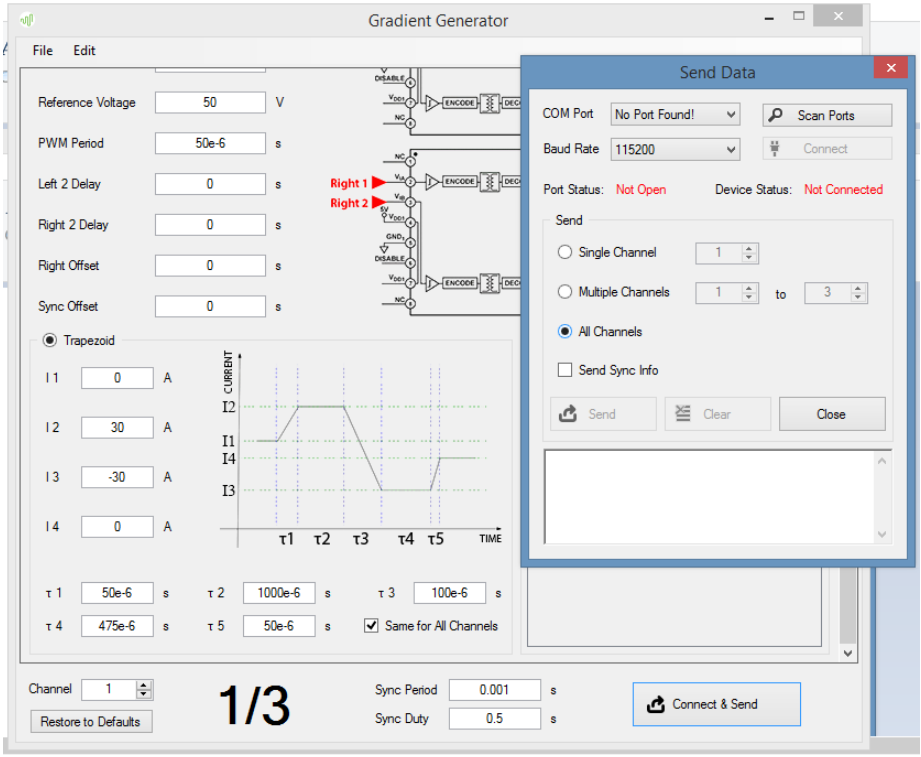

(b)

Figure 2.10: Developed user-interface to specify load, current (a) and timing parameters (b) for each channel independently.

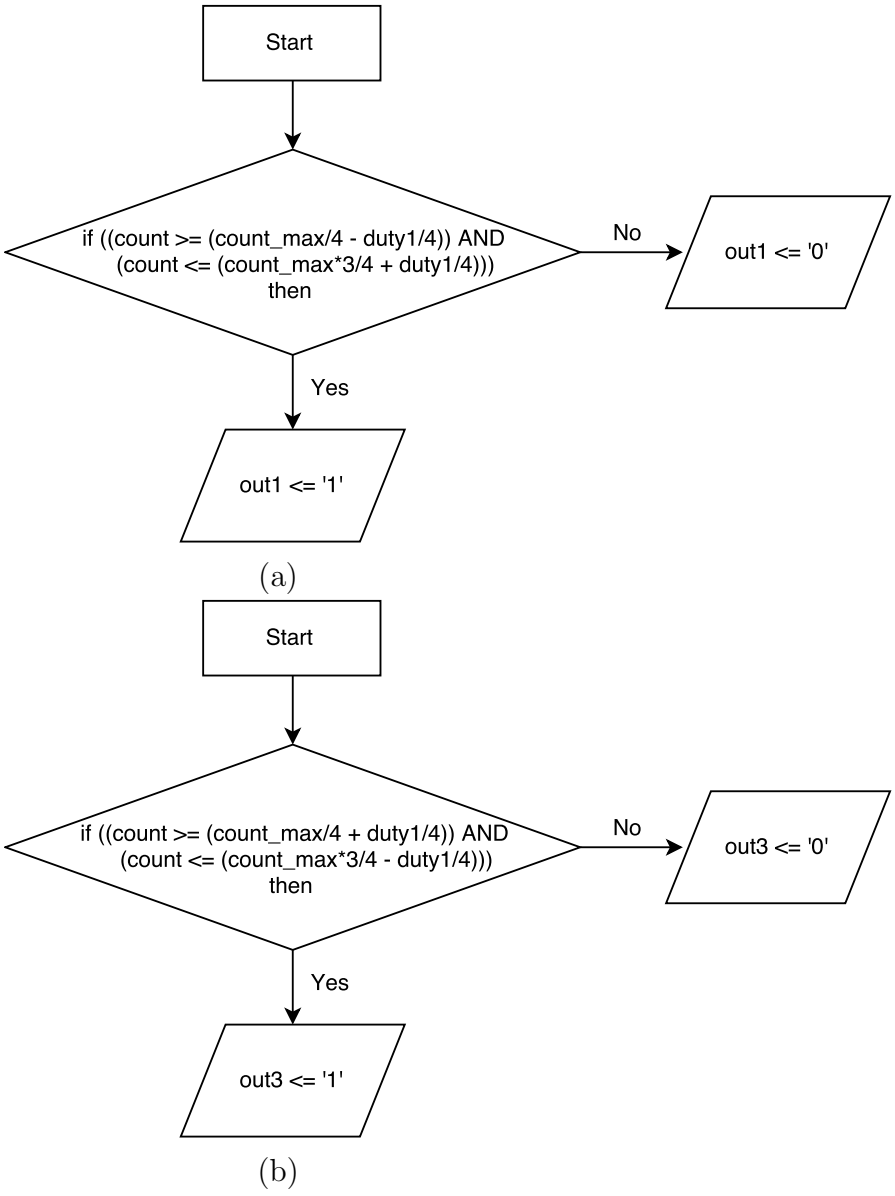

Figure 2.11: Signal generation flow chart for D^+(a) and D^-(b) duty cycles for $Q1$ and $Q3$ switches, respectively.

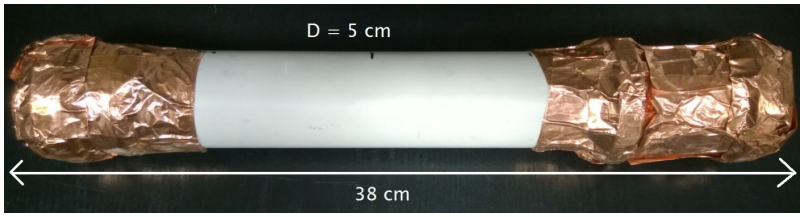

Figure 2.12: Cylindrical phantom shielded to prevent excitation of unwanted regions.

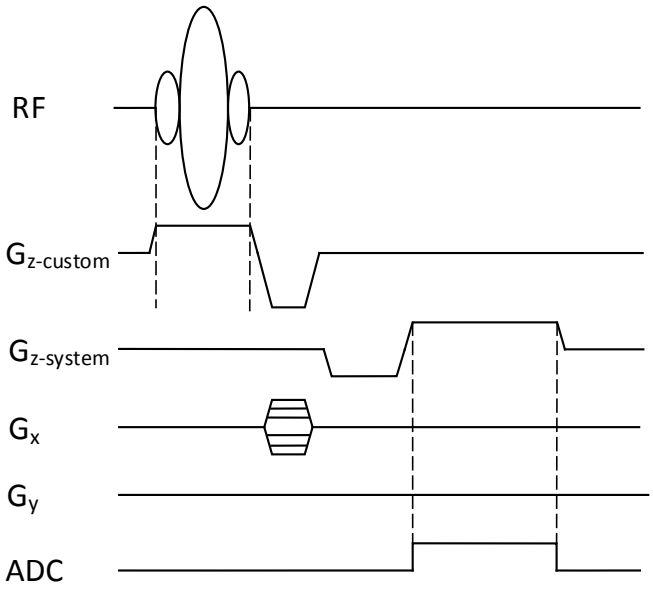

Figure 2.13: Pulse sequence for 2D slice selection using custom coil and read-out using system gradient.

Chapter 3

Results

Simulations and experiments were conducted to evaluate the performance of this gradient system. The coil array simulation results are presented in the following section. Output testing of the FPGA and the GPAs was done separately by monitoring PWM signals and trapezoidal current waveform flowing in the coil before inserting in the scanner. Phantom experiments and slice selection images are depicted in the last section of this chapter. Simulation and experimental results are discussed in the next chapter.

3.1 Simulation Results

For this system, the ratio of the currents between the outer, middle and the inner channels found to be 3.1 : 2.3 : 1 A in order to obtain maximum size of VOI. For the current ratio of 0 : 3.1 : 1 smaller VOI is achieved while the outer channel is not used. As the third case, when only the inner channel is used, smallest linear region with higher slew-rate will be available. Fig. 3.1 shows simulation results for the generated magnetic field from each channel with spacing and current values mentioned before for each size of VOI. It can be observed that for large VOI (Fig. 3.1(a)) the combination of the generated fields by each channels results in a

linear field variation across the volume. For mid-size VOI (Fig. 3.1(b)), the field generated by the inner channel corrects the nonlinearities of the middle channel. The field generated by the inner channel is linear around the center and in a small region and no need to correction (Fig. 3.1(c)). So by maintaining these current ratios, different sizes of VOI is achievable.

Fig. 3.2 depicts the maximum magnetic and gradient field for different sizes in simulation applying maximum current of 30 A. For the large VOI, maximum magnetic field value is about 10 mT and generated gradient field is about 125 mT/m compared to mid-size case with 8mT and 125 mT/m, respectively which shows smaller magnetic field peak for same gradient strength. This gives us more flexibility in terms of PNS limitations. For the smallest VOI, although the gradient strength is about two times of the other cases, the magnetic field peak value is 6.5 mT. Maximum achievable gradient strength is acquired in small VOI, hence according to the application desired combination can be selected. Gradient field variations in VOI is less than 5% which is generally considered as maximum allowable nonlinearity in gradient systems. The length of these regions for large, mid-size and small one are about 12.5, 10 and 2.5 cm accordingly.

In addition to linearity along cylinder axis (z), field properties should be uniform in the VOI along the x and y axis. Fig. 3.3 shows magnetic field in the yz plane for the optimal current ratios mentioned above in simulation for three cases. The oval VOI with 95% uniformity for each mode is specified. In all cases the maximum width of the VOI is about 3.4 cm which is located at the center of the coil (z=0). Since the coil geometry is symmetric about its axis, field properties will be constant in ϕ direction.

3.2 Hardware Implementation and Experiment Results

The PWM signals for the high side MOSFET in each half-bridge generated by the FPGA is given in Fig. 3.4. Desired duty cycle calculated by the Eq. 2.3 and 2.4 is consistent with measured duty cycle at the output of the FPGA. Figure 3.5 shows the PWM pulses required to have trapezoidal current waveform and the floating voltages at the output of the GPA with 50 V line voltage. Comparing Fig. 3.4 and 3.5 reveals that pulses at the GPA output, precisely follows the FPGA output in terms of timing and pulse shapes.

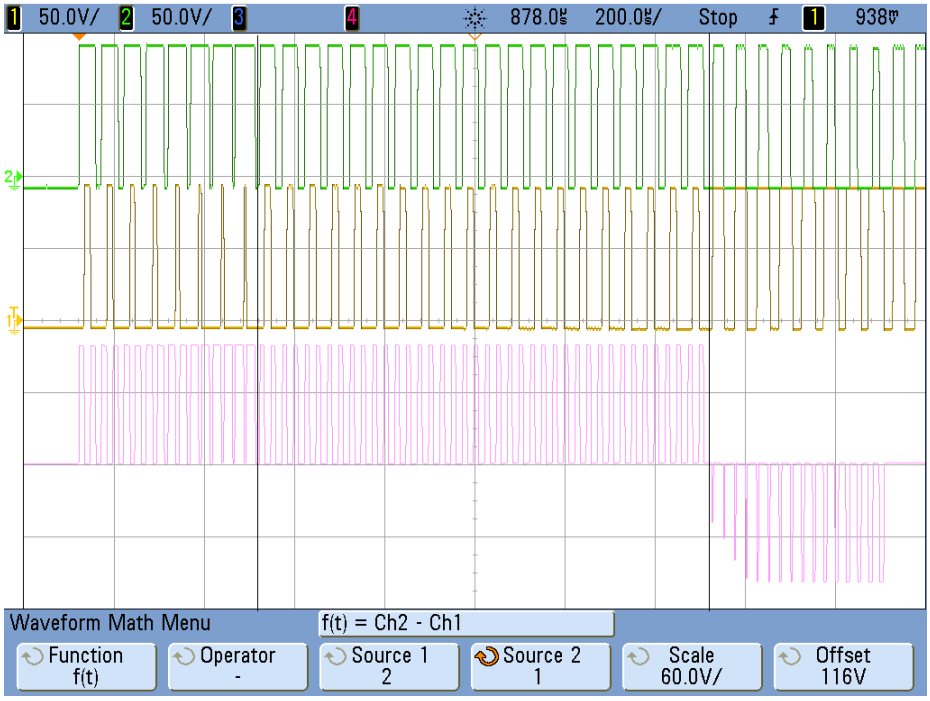

Figure 3.5: Floating Voltage at the output of the GPA (Ch1, Ch2) and their subtraction (bottom) as PWM pulses seen by the load.

We were able to drive our coil with 30 A maximum current as shown in Fig. 3.6, measured with a current probe with 10 A/mV scale. There is a ripple about 5% of the maximum value present on the current waveform which is inherent in switching amplifiers. Rising and falling times are equal to 40 μs and flat top

duration is 800 μs.

After measuring current and voltage on the load and input of the amplifier, output and input average power calculated in MATLAB are 12.5 W and 26.3 W, respectively. In addition, 0.49 W power consumption in driving circuit, gives efficiency of 46.6%. Although this value is not high considering common H-bridge

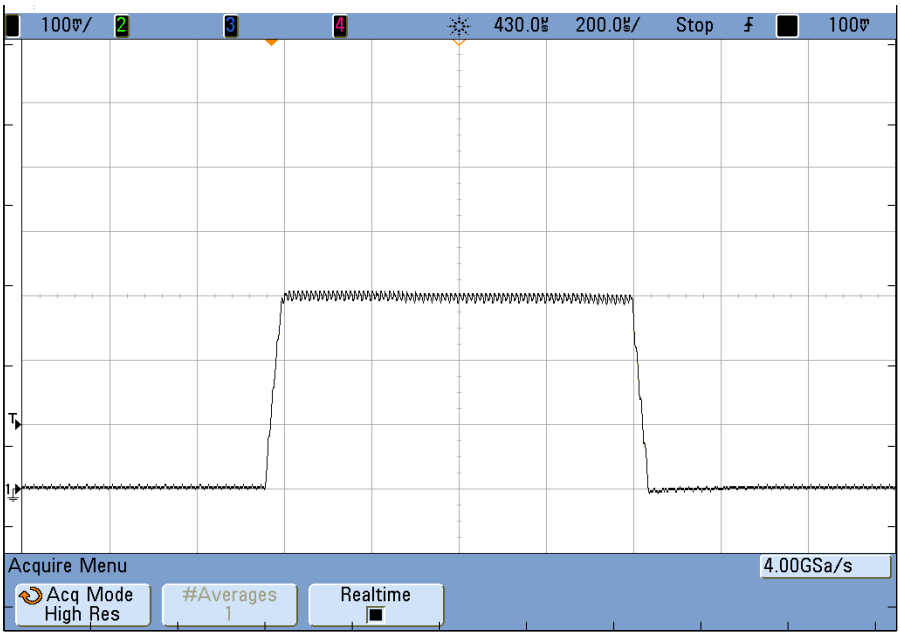

Figure 3.6: Measured current waveform passing through the custom coil by a current probe at 10 mV/A.

amplifiers, but it can be legitimized by the following explanation. Ideally there should not be any losses in inductive load at the output, but in practice there is a resistance of the conductor which in our case is about 390 $m\Omega$. According to the data sheet, each of the MOSFET switches in the H-bridge has "on resistance" ($R_{DS(on)}$) of about 0.075 Ω and in each cycle two ON switches are in current path results in about 0.15 Ω which may be practically higher and almost is comparable with the load resistance. As a result considering switching and driver circuit losses with less contribution to overall loss, efficiency value falls in the range declared above. In other words, for an efficient H-bridge amplifier design with lowest possible loss, MOSFET selection as switch with low $R_{DS(on)}$ and switching losses

is important, since they are responsible mechanisms for most of the losses in the circuit.

In order to experimentally achieve high efficiency using our custom GPA, we drive the other coil built specifically for this purpose. This coil has 730 μH inductance and 1.82 Ω resistance as mentioned before and we could drive that with 26 A current at the flat top [Fig. 3.7]. Rising and falling durations are equal to 400 μs and 1 ms flat top duration which requires 95 V hence 95% maximum duty cycle for 100 V line voltage. Fig. 3.8 shows the current waveform and voltage at the input of the amplifier with maximum available current on the load. In order to measure efficiency of the GPA with this load, input and output powers calculated in MATLAB using data in Fig. 3.7 and 3.8 to be 143 W and 132 W, respectively. So total power of 11 W is dissipated in the H-bridge switches which includes MOSFET conducting losses due to $R_{DS(on)}$ and switching losses. Switching losses are frequency dependent and increase with higher switching frequencies. For the working frequency of this system (100 KHz) switching losses seems to be negligible compare to conducting losses. Driver circuit power consumption is less than 1 W hence negligible. For this case efficiency is about 92 % which is expected according to the transistor's on resistance and resistance of the load which is calculated as follow:

$$\eta = \frac{R_L}{R_L + R_{DS(on)}} = \frac{1.82}{1.82 + 2 \times 0.75} \times 100 = 92.4\% \tag{3.1}$$

In Fig. 3.8, during ramp up time, 1, some of required power is provided by capacitors at the input of the GPA, since high power is necessary in this duration. In regions 2 and 3 sine high power requirements is less, power supply starts to provide the load with sufficient current values at flat top and ramp down regions. After that, it charges the capacitor of the GPA again, resulting this current waveform. As stated before, this coil was built to only examine the efficiency of the GPA in its high power margins.

Magnetic field amplitude measured and its derivative calculated to evaluate achieved linearity by three channel coil, both are depicted in Fig. 3.9. Linear field is achieved for three cases as well for average current values of $0.29 : 0.2 : 0.11$,

$0 : 0.26 : 0.09$ and $0 : 0 : 0.15$ A for outer, middle and inner channel for (a), (b) and (c), respectively. Low current values used in order to prevent fast dephasing of the echo signal. The difference between current ratios in practice and simulation most probably comes from measuring error of the current probe ($\sim$50 mA) and also small mismatch (3.5 mm) between loops width and their locations in prototype and simulation. It can be observed that overall characteristic of magnetic field exactly matches with simulation. Since we didn't place any indicator on the phantom as location reference, exact information about the length of the linear field couldn't be extracted, but it is similar to simulation results. ΔG in linear region is about 1.02, 0.73 and 0.2 mT for (a), (b) and (c), respectively. Gradient efficiency for these three combinations are roughly 13.3, 20.6 and 53.3 $\mathrm{mT/m/A_{avg}}$. Note that average current value is used in these calculation. Sharp oscillations in field derivative is measured noise along with magnetic field values.

Fig. 3.10 shows measured magnetic field in yz plane for optimum current ratios mentioned above for for (a), (b) and (c), respectively. Field homogeneity in y direction (and symmetrically in x direction) and linear volume along the z axis matches with simulations as well.

Maximum generated gradient strength applying highest available current to the channels to acquire a 2D slice at the center of the coil along with center line plot for each mode is depicted in Fig. 3.11 from top to bottom row for large, mid-size and small VOI, respectively with fixed RF duration of 800 μs. Gradient strength and slice thickness are equal for large and mid-size VOI. However, required and dissipated overall power is smaller for second case, because of decreased number of channels and GPAs used. On the other hand, since there is no mutual coupling between middle and outer coil in mid-size case, required voltage for second channel is smaller for this region compared to large one. If small VOI is needed according to the application, gradient strength gets almost doubled and also required and dissipated power decreased as expected.

Fig. 3.12 shows operation of gradient array considering PNS. For fixed RF duration and almost same slice thickness, magnetic field maximum value which is

the effective parameter in PNS limitation, is changing. Hence, acquiring images can be done optimized for PNS according to the required size of VOI.

Properties for each mode can be extended to off-center slices as well. Some sample slices also selected along the phantom for different VOI sizes as depicted in Fig. 3.13 with FOV=200x62 mm and same gradient strength and RF duration.

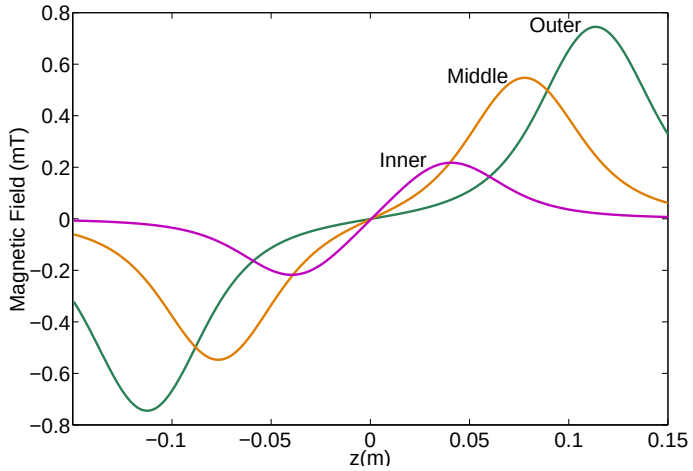

(a)

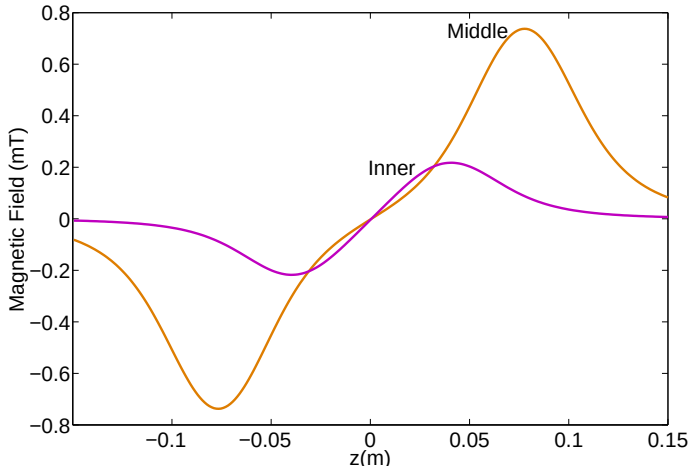

(b)

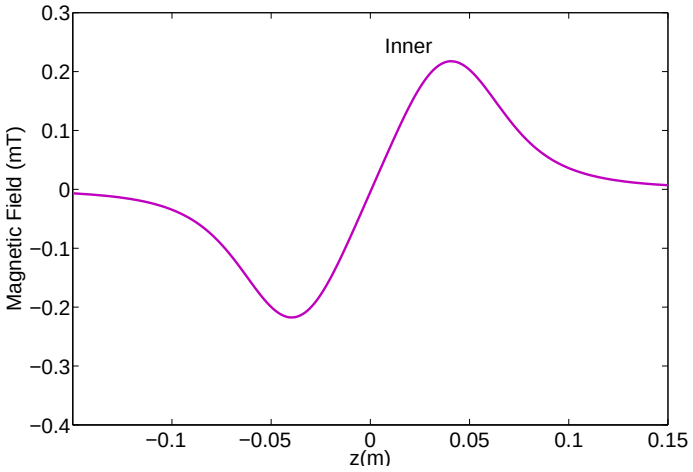

(c)

Figure 3.1: Magnitude of the generated magnetic field by each channel on the z axis which results in overall linear field with currents of 3.1 : 2.3 : 1 A (a), 0 : 3.1 : 1 A (b) and 0 : 0 : 3.1 A (c) for outer, middle and inner channels, respectively.

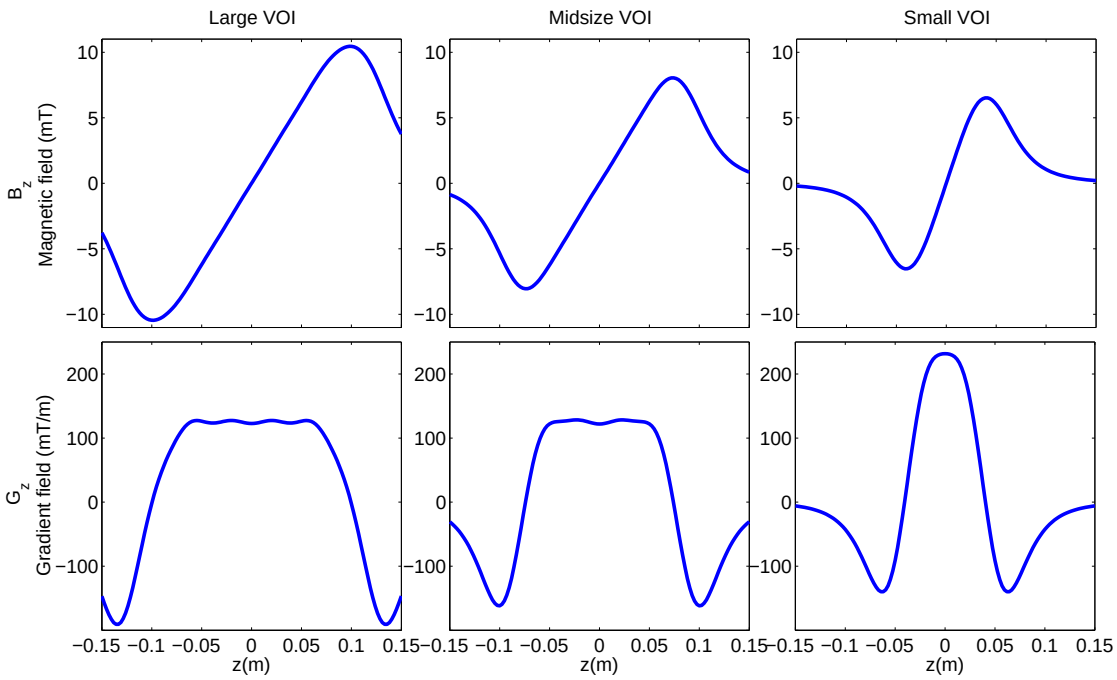

Figure 3.2: The magnetic field and its derivative on the z axis with a: currents ratios of 3.1 : 2.3 : 1 A, b: 0 : 3.1 : 1 A, c: 0 : 0 : 3.1 A for outer, middle and inner channels, respectively applying 30 A as maximum current.

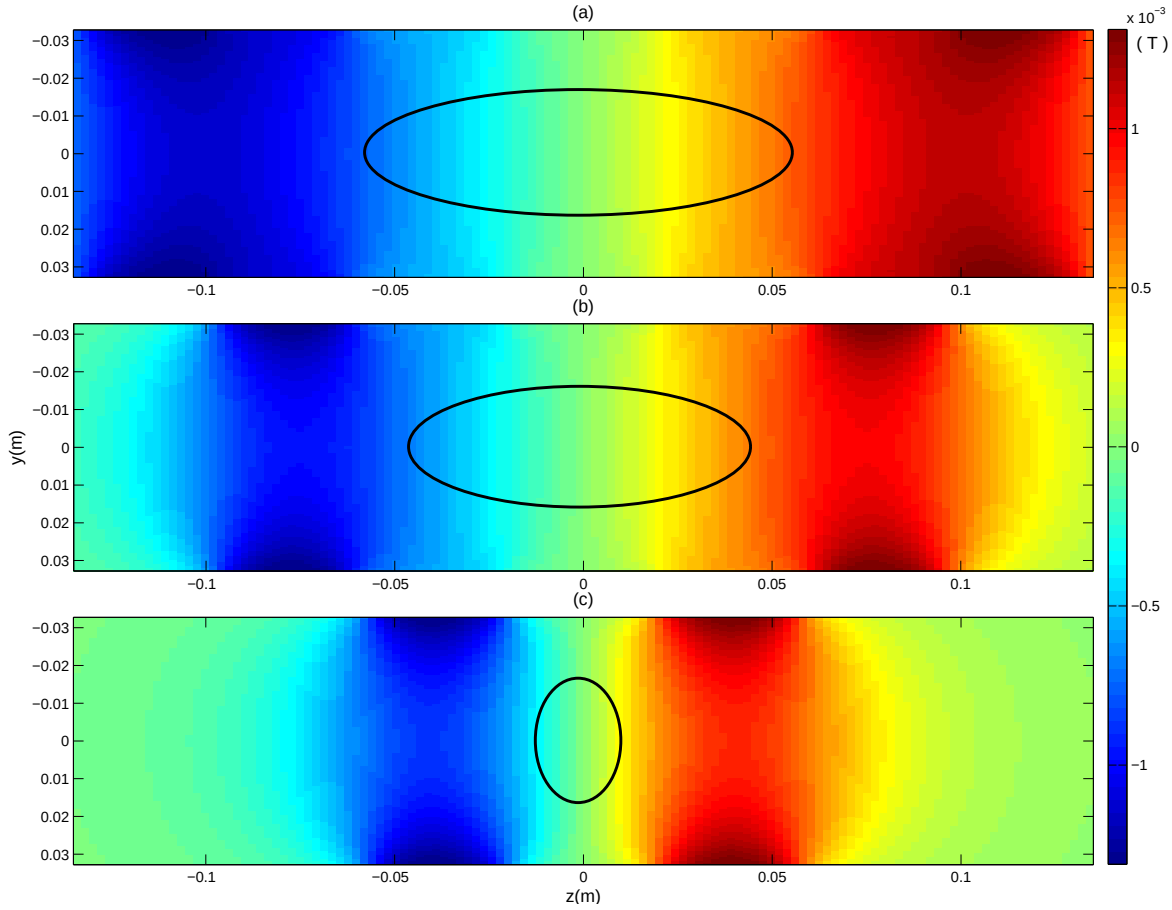

Figure 3.3: Linear magnetic field in yz plane for 587 cm^3 (a), 441 cm^3 (b) and 110 cm^3 (c) of VOI.

Figure 3.4: PWM pulses at the output of the FPGA for left (Ch1) and rigth (Ch2) half-bridges for high side switches and their subtraction as desired duty cycle (bottom) for a trapezoidal current.

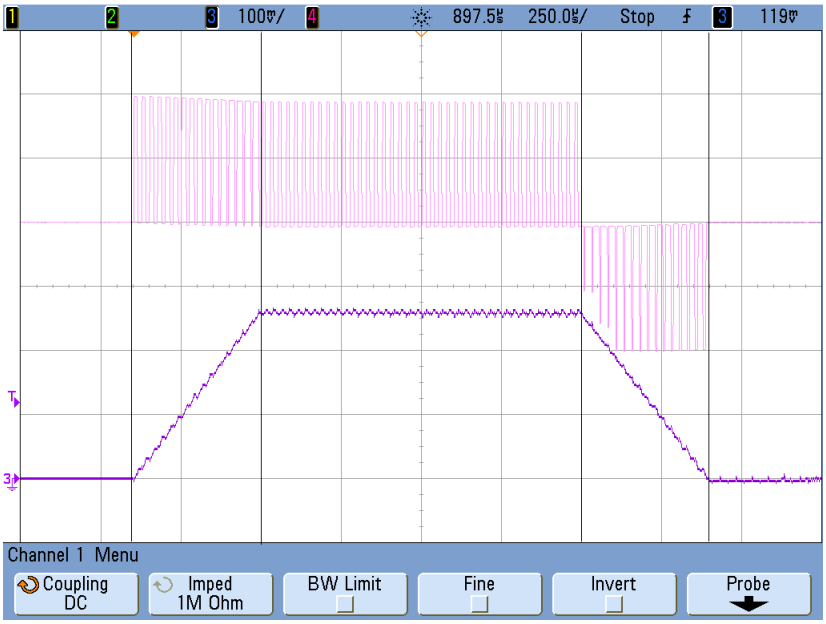

Figure 3.7: Measured current and voltage of a coil with 730 μH inductance and 1.82 Ω resistance and 26 A flat top current value.

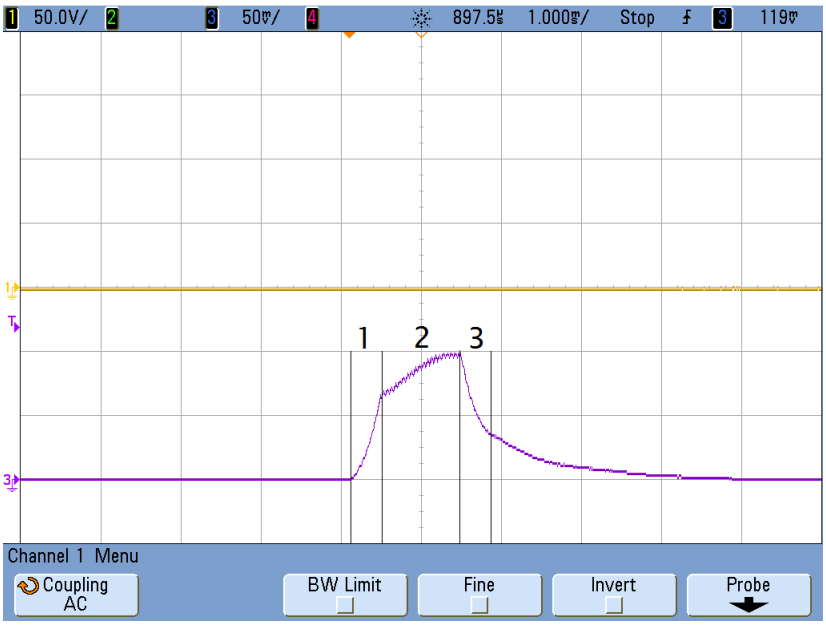

Figure 3.8: DC voltage (100 V) and current waveform ($10mV/A$ scale)at the input of the GPA, while driving the coil with 730 μH inductance and 1.82 Ω resistance by 26 A flat top current, with specified ramp up, flat top and ramp down regions as 1, 2 and 3, respectively.

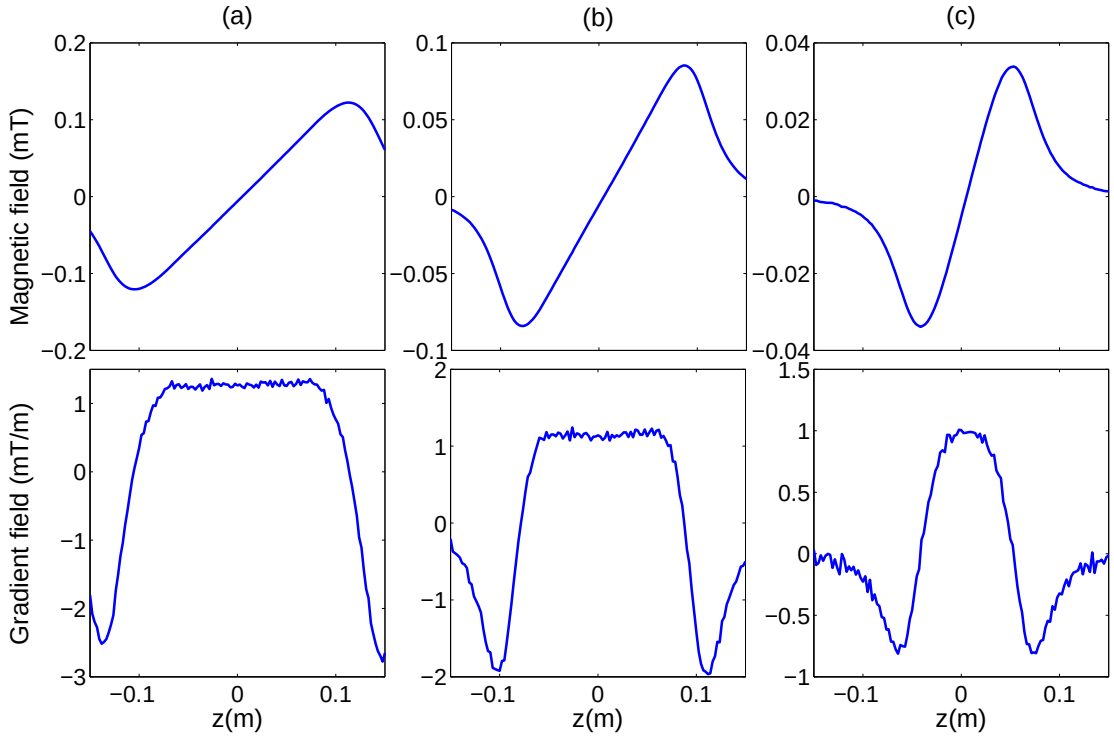

Figure 3.9: Measured magnetic fields and its derivative for a: $0.29 : 0.2 : 0.11$ A, b: $0 : 0.26 : 0.09$ A, c: $0 : 0 : 0.15$ A for outer, middle and inner channels, respectively.

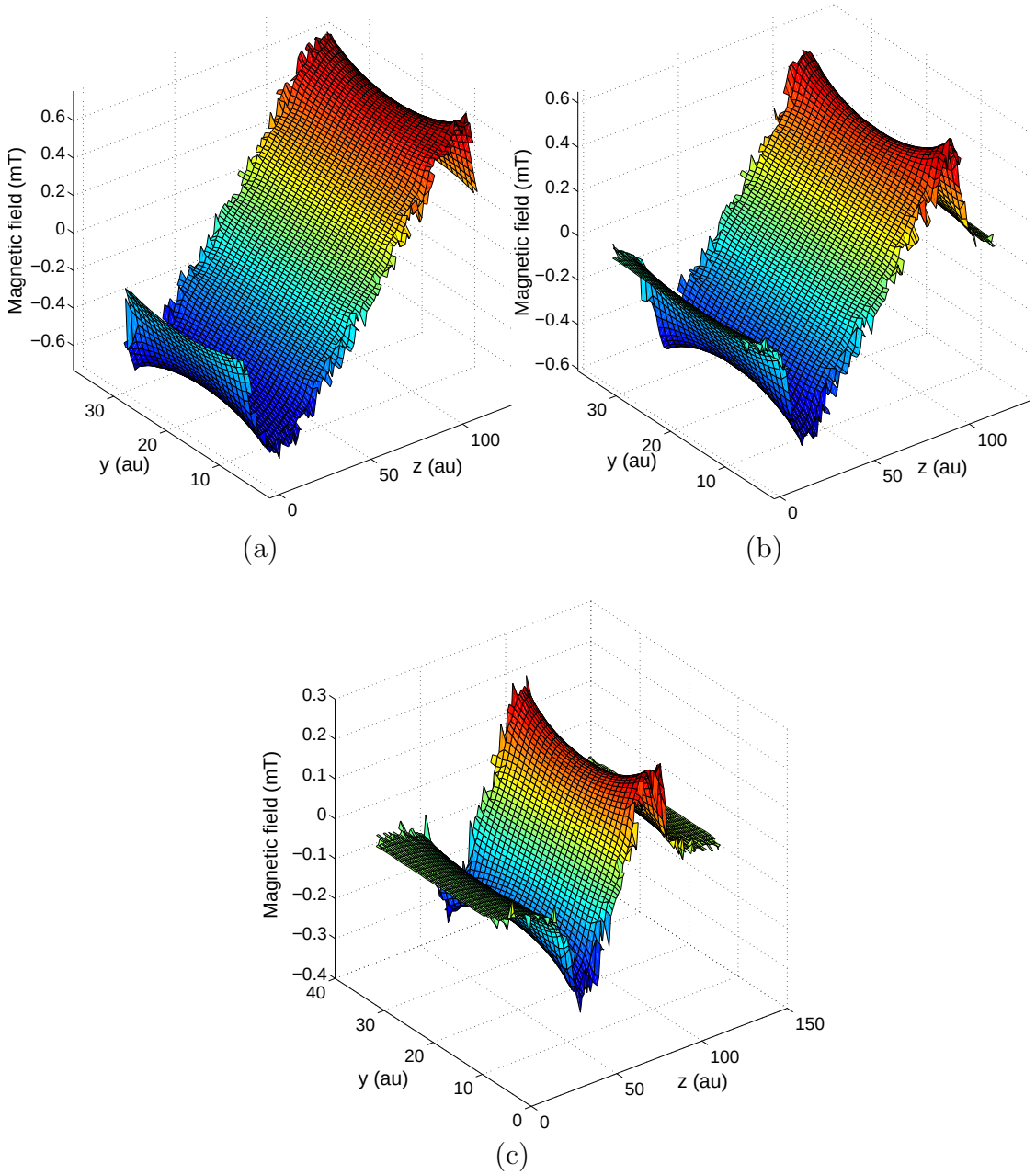

Figure 3.10: Measured magnetic field amplitude in yz plane for a: $0.29 : 0.2 : 0.11$ A, b: $0 : 0.26 : 0.09$ A, c: $0 : 0 : 0.15$ A for outer, middle and inner channels, respectively with variable VOI similar to the simulation.

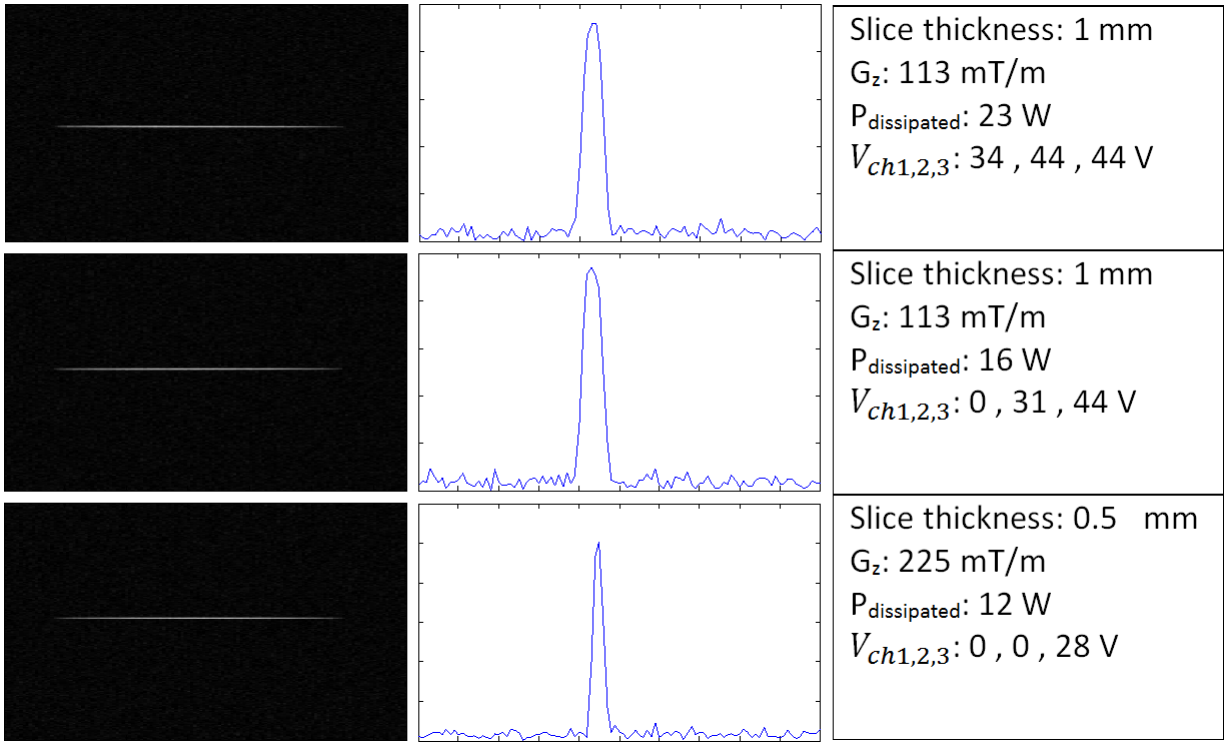

Figure 3.11: 2D coronal slice selection at xy plane along with center line plot and properties of each mode from top to bottom for large, mid-size and small VOI with fixed RF duration (800 μs).

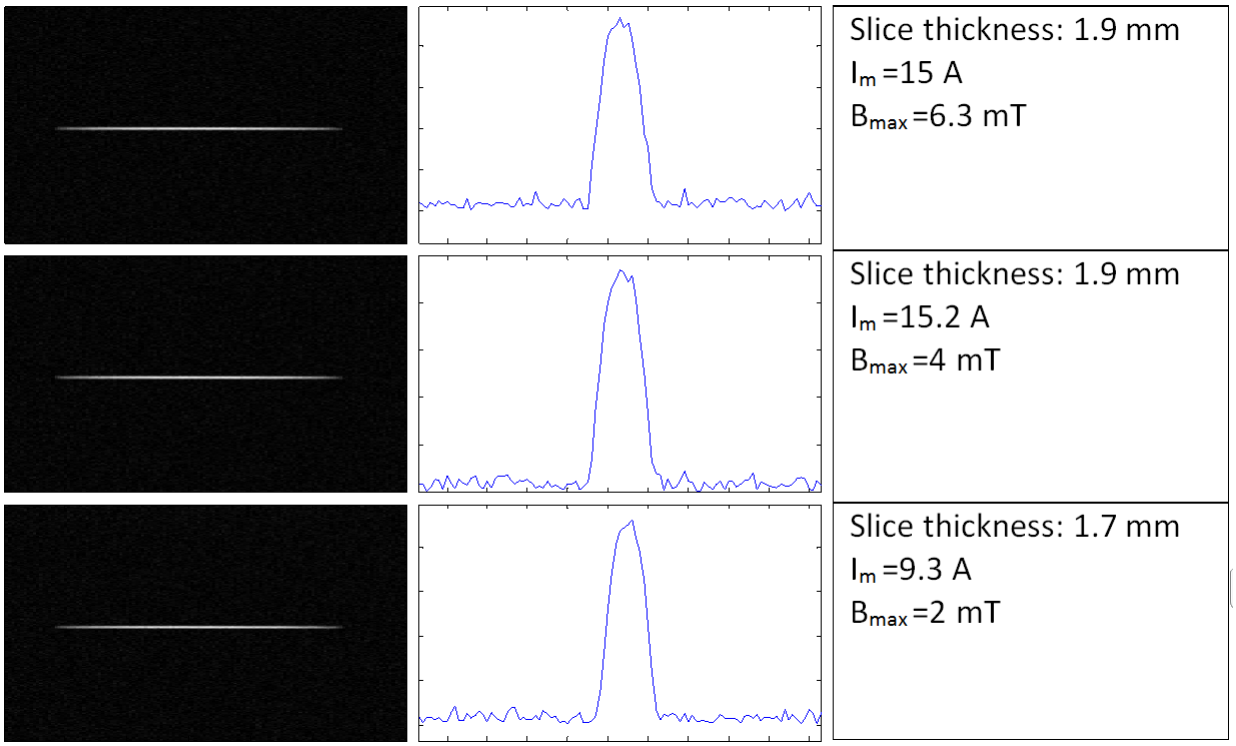

Figure 3.12: 2D coronal slice selection at xy plane along with center line plot for almost equal slice thickness from top to bottom for large, mid-size and small VOI with fixed RF duration (800 μs) showing B_{max} change for each case.

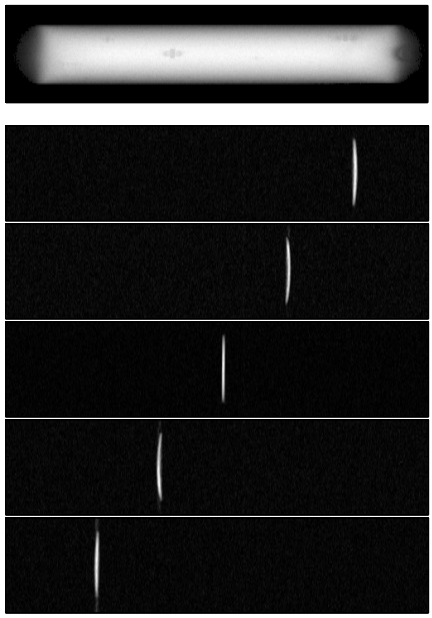

(a)

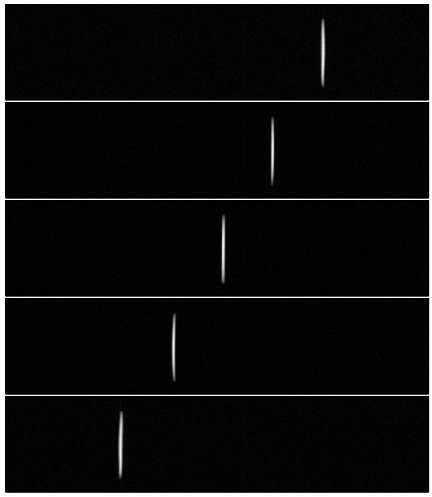

(b)

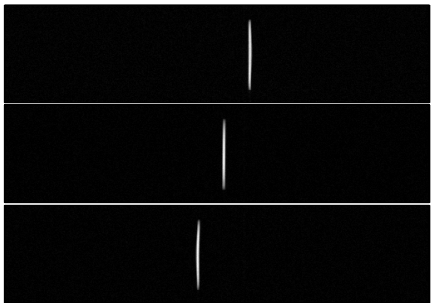

(c)

Figure 3.13: Off-center slice selection of the phantom for a: large, b: mid-size and c: small VOI with FOV=200x62 mm.

Chapter 4

Discussion and Conclusion

This study demonstrates the feasibility of proposed method to generate gradient fields in z-direction using gradient array and independent GPAs. The ability of achieving proper current density distribution on the surface of a cylinder using coil array has been shown, which is capable to generates desired linear magnetic field in different sizes of VOI. Measurement results are in accordance with the simulations. Independent coil channels with dedicated GPAs introduce high flexibility to the system in terms of mixing the fields according to the application. High gradient is achievable observing PNS limitations as well for smaller VOI. Also conventional larger VOI is available for whole body imaging. An FPGA controls the GPAs that are driving the coils in a precise manner.

Harvey's proposed "twin coil" gradient system [21] consists of two sets of three channel coils and one three channel GPA. Each set of coils are connected to the amplifier using a switching network. Flexibility in acquiring two size of VOI is achieved at the cost of reduced patient bore diameter since two sets are placed at separate layers of a cylindrical former and still using one amplifier for a unite coil in each direction.

Continuous variable field characteristic system [25], is composed of two sets of three channel coil sharing a common surface, two three-channel amplifier and

six channel gradient controller. This design suffers from reduced field efficiency for small ROI and there is no structural modification in driver system, using one GPA for whole coil in each direction.

Combination of these two systems somehow can be done through presented work and benefit from advantages of both designs. In this work the partitioned coils are winded on the same former so no reduction in patient bore size. Since the inner coil also has enough turn number, even small current values can generate high magnetic field with high field efficiency. Also since there is a dedicated amplifier for each coil, no switching mechanism is needed.

Partitioning the coil into several coils with lower inductance is less demanding in terms of voltage requirements for the GPAs, thus the amplifiers can be both less expensive and complicated. Although we didn't optimize three channel coil for high efficiency considering our GPA, the other one channel coil built for this purpose, revealed high efficiency in high power margins. There are two mainstreams responsible for high efficiency, lower on-resistance of switches ($R_{DS(on)}$) or higher resistance of the load. Each of these parameters can be optimized according to the specific coil or amplifier.

Throughout the slice selection, we used system body coil for readout which excites unintended regions as well and in order to prevent that, phantom was shielded by copper foil. However this can be solved by adapting the size of the transmit coil to VOI by the help of proper RF transmit array along with gradient array system.

Obtained results are promising and for implementation of this design in a clinical MRI scanner much more work needs to be carried out. Amplifier design can be improved for lower loss and higher current capabilities. Also a feedback system can be integrated in order to adjust the current more precisely, hence more accurate magnetic field. At this stage we didn't use any filtering modalities to cancel the ripples that naturally are present in H-bridge output current for inductive load. Mutual coupling between coils can be used as an advantage to cancel out overall ripples by using PWM pulses with shifted phases with respect

to each other which will be considered in future. Arbitrary current waveform implementation and load specifications can be adjusted on FPGA board and all the calculations are done in FPGA which are computationally heavy. More friendly user-interface and implementing developed Micro-Blaze core are under investigation for higher number of channels. Regarding gradient coils we didn't use any optimization method for optimal geometry of the coil windings, their inductance, conductor resistance, higher field generation and shielding methods. In this work linear field was of concern, but increasing number of the channels gives us more flexibility in generation of linear and also non-linear fields. We have not tested the gradient array for x- and y-gradients. Although we managed to deal with mutual coupling between the coil elements, it is now known what kinds of problems we may face in a whole body gradient array design. For multiple independent gradient coils, cabling can be an issue, however, since applied voltage rate are reduced, cables with narrower isolation can handle the voltage and current, thus less increase in overall cable diameter will be required. Since broad research is conducting on various fields in MRI, and the fundamental needs regarding gradient system efficiency and operation, further improvements in these systems are expected sooner or later.

Bibliography

[1] R. Turner, "Gradient coil design: a review of methods," *Magnetic Resonance Imaging*, vol. 11, no. 7, pp. 903–920, 1993.

[2] R. Turner, "A target field approach to optimal coil design," *Journal of physics D: Applied physics*, vol. 19, no. 8, p. L147, 1986.

[3] M. W. Garrett, "Axially symmetric systems for generating and measuring magnetic fields. part i," *Journal of Applied Physics*, vol. 22, no. 9, pp. 1091–1107, 1951.

[4] P. B. Roemer and J. S. Hickey, "Self-shielded gradient coils for nuclear magnetic resonance imaging," Apr. 12 1988. US Patent 4,737,716.

[5] P. Mansfield, B. L. Chapman, R. Turner, and R. M. Bowley, "Magnetic field screens," Dec. 18 1990. US Patent 4,978,920.

[6] B. Suits and D. Wilken, "Improving magnetic field gradient coils for nmr imaging," *Journal of Physics E: Scientific Instruments*, vol. 22, no. 8, p. 565, 1989.

[7] R. Turner, "Minimum inductance coils," *Journal of Physics E: Scientific Instruments*, vol. 21, no. 10, p. 948, 1988.

[8] R. Lai, J. Sabate, S. Chi, and W. Skeffington, "High performance gradient driver for magnetic resonance imaging system," in *Energy Conversion Congress and Exposition (ECCE), 2011 IEEE*, pp. 3511–3515, IEEE, 2011.

[9] R. L. Steigerwald and W. F. Wirth, "High-power, high-performance switching amplifier for driving magnetic resonance imaging gradient coils," in

Power Electronics Specialists Conference, 2000. PESC 00. 2000 IEEE 31st Annual, vol. 2, pp. 643–648, IEEE, 2000.

[10] J. Sabate, L. J. Garces, P. M. Szczesny, Q. Li, and W. F. Wirth, "High-power high-fidelity switching amplifier driving gradient coils for mri systems," in *Power Electronics Specialists Conference, 2004. PESC 04. 2004 IEEE 35th Annual*, vol. 1, pp. 261–266, IEEE, 2004.

[11] J. Sabate, L. Garces, P. Szczesny, Q. Li, and W. F. Wirth, "High-bandwidth high-power gradient driver for magnetic resonance imaging with digital control," in *Applied Power Electronics Conference and Exposition, 2005. APEC 2005. Twentieth Annual IEEE*, vol. 2, pp. 1087–1091, IEEE, 2005.

[12] P. Mansfield, A. Blamire, R. Coxon, P. Gibbs, D. Guilfoyle, P. Harvey, M. Symms, J. Waterton, P. Bottomley, A. Garroway, *et al.*, "Snapshot echo-planar imaging methods: Current trends and future perspectives [and discussion]," *Philosophical Transactions of the Royal Society of London A: Mathematical, Physical and Engineering Sciences*, vol. 333, no. 1632, pp. 495–506, 1990.

[13] P. Mansfield and P. Harvey, "Limits to neural stimulation in echo-planar imaging," *Magnetic resonance in medicine*, vol. 29, no. 6, pp. 746–758, 1993.

[14] W. Irnich and F. Schmitt, "Magnetostimulation in mri," *Magnetic resonance in medicine*, vol. 33, no. 5, pp. 619–623, 1995.

[15] P. R. Harvey and P. Mansfield, "Avoiding peripheral nerve stimulation: Gradient waveform criteria for optimum resolution in echo-planar imaging," *Magnetic resonance in medicine*, vol. 32, no. 2, pp. 236–241, 1994.

[16] T. F. Budinger, H. Fischer, D. Hentschel, H.-E. Reinfelder, and F. Schmitt, "Physiological effects of fast oscillating magnetic field gradients.," *Journal of computer assisted tomography*, vol. 15, no. 6, pp. 909–914, 1991.

[17] C. Ham, J. Engels, G. Van de Wiel, and A. Machielsen, "Peripheral nerve stimulation during mri: effects of high gradient amplitudes and switching rates," *Journal of Magnetic Resonance Imaging*, vol. 7, no. 5, pp. 933–937, 1997.

[18] R. M. Vavrek and C. C. Myers, "Multiple tap gradient field coil for magnetic resonance imaging," May 10 1994. US Patent 5,311,135.

[19] E. Katznelson and P. Harvey, "Modular whole-body gradient coil comprising first and second gradient coils having linear gradients in the same direction," Apr. 7 1998. US Patent 5,736,858.

[20] P. R. Harvey and E. Katznelson, "Modular gradient coil: A new concept in high-performance whole-body gradient coil design," *Magnetic resonance in medicine*, vol. 42, no. 3, pp. 561–570, 1999.

[21] P. R. Harvey, "The modular (twin) gradient coil?high resolution, high contrast, diffusion weighted epi at 1.0 tesla," *Magnetic Resonance Materials in Physics, Biology and Medicine*, vol. 8, no. 1, pp. 43–47, 1999.

[22] P. R. Harvey, "The modular gradient coil: an holistic approach to power efficient and high performance whole-body mri without peripheral nerve stimulation," *Magnetic Resonance Materials in Physics, Biology and Medicine*, vol. 9, no. 3, pp. 152–155, 1999.

[23] C. L. Ham, G. B. Mulder, and G. N. Peeren, "Magnetic resonance imaging apparatus including a graident coil system with a correction coil," May 22 2001. US Patent 6,236,208.

[24] Y. M., "Mr imaging device," 1999. 1,122,1200.

[25] R. Kimmlingen, M. Gebhardt, J. Schuster, M. Brand, F. Schmitt, and A. Haase, "Gradient system providing continuously variable field characteristics," *Magnetic resonance in medicine*, vol. 47, no. 4, pp. 800–808, 2002.

[26] M. Vlaardingerbroek and J. Boer, "Magnetic resonance imaging: Theory and practice," Physics and astronomy online library, Springer, 2003.

[27] S. Hidalgo-Tobon, "Theory of gradient coil design methods for magnetic resonance imaging," *Concepts in Magnetic Resonance Part A*, vol. 36, no. 4, pp. 223–242, 2010.

[28] H. Wheeler, "Formulas for the skin effect," *Proceedings of the IRE*, vol. 30, pp. 412–424, Sept 1942.

[29] E. Rosa and F. Grover, *Formulas and tables for the calculation of mutual and self-inductance*. U.S. Dept. of Commerce and Labor, Bureau of Standards, 1912.

[30] F. Schmitt, "The gradient system.,"

[31] A. MiniKit, "H-bridge driver circuit using isolated half-bridge drivers,"